2010-08-12

Synthesis and Characterization of an Oligothiophene-Ruthenium Complex and Synthesis and Optical Properties of Oligothiophene-Ruthenium Complexes Bound to CdSe Nanoparticles

Nathan A. Bair
Brigham Young University - Provo

Synthesis and Characterization of an Oligothiophene-Ruthenium Complex and Synthesis and Optical Properties of Oligothiophene-Ruthenium Complexes Bound to CdSe Nanoparticles

Nathan Bair

A thesis submitted to the faculty of
Brigham Young University
in partial fulfillment of the requirements for the degree of

Master of Science

Roger G. Harrison, Ph.D.
Matthew C. Asplund, Ph.D.
Merritt B. Andrus, Ph.D.
John D. Lamb, Ph.D.

Department of Chemistry and Biochemistry

Brigham Young University

December 2010

ABSTRACT

Synthesis and Characterization of an Oligothiophene-Ruthenium Complex and

Synthesis and Optical Properties of Oligothiophene-Ruthenium

Complexes Bound to CdSe Nanoparticles

Nathan Bair

Department of Chemistry and Biochemistry

Master of Science

Abstract

Oligothiophenes are of increasing interest in organic based electronic devices in part due to their high electron and hole mobilities. In an organic photovoltaic (OPV) device, the electronic properties of oligothiophenes make them advantageous as charge transfer junctions. To serve as charge transfer junctions, oligothiophenes must be functionalized to bind to the donor and acceptor parts of the device. The donor and acceptor parts are different materials and the synthesis of asymmetric oligothiophenes is of great interest. Previous researchers in our lab synthesized four asymmetric oligothiophenes, two with two thiophene subunits and two with four. Each set of oligothiophenes contained a pair of constitutional isomers. Here we report the synthesis of another asymmetric oligothiophene, one with three thiophene subunits. This compound is functionalized with bipyridine to bind $Ru(bpy)_2^{2+}$ and with phosphonic acid moieties to bind CdSe nanoparticles. The synthesis was carried out by bonding a phosphonic acid moiety to bithiophene and bipyridine to thiophene and then coupling the phosphate-bithiophene and thiophene-bipyridine. Standard Stille couplings were used for carbon-carbon bond formation. The resulting compounds have complex NMR spectra and overlapping Ru MLCT and π- π^* transitions at 450 nm with molar extinction coefficient on the order of 3×10^5 M^{-1} cm^{-1}. The thiophene fluorescence is quenched by $Ru(bpy)_2^{2+}$. These optical properties compare closely with the previous compounds synthesized.

Abstract

Solar cells occupy significant attention in the media, politics and science for their promise of continual pollution-free energy. Quantum dots, metal complexes and organic compounds are all under research as viable replacements for expensive silicon solar cells. To test the efficacy of a light harvesting compound before constructing a solar cell, a model system is constructed to show electron transfer from the light harvester into an electron acceptor. We

synthesized oligothiophenes and oligothiophene-ruthenium complexes and tested their ability to act as sensitizers and charge transfer junctions. To do this, they were bonded to CdSe nanoparticles and their optical properties were measured. Steady-state photoluminescence and time correlated single photon counting were used to observe the effects on fluorescence and fluorescence lifetime of the CdSe-oligothiophene and CdSe-oligothiophene-ruthenium complexes before and after binding. It was found that CdSe fluorescence was quenched when bound to an oligothiophene ruthenium complex, and that the fluorescence of the oligothiophene was quenched when bound to CdSe in the absence of ruthenium. The fluorescence lifetimes of the quenched species were shortened.

Keywords: [Oligothiophene, CdSe nanoparticle, Ruthenium]

ACKNOWLEDGEMENTS

I would like to thank Dr. Harrison for his patience and perseverance, Sarah for her selflessness and endless support, and my parents and family who are largely responsible for guiding me to where I am today.

Contents

1.1. Introduction

Organic solar cells are named for the use of an organic donor compound in the active layer (Figure 1.1). The donor material is commonly an organic polymer, conjugated or aromatic oligomer, or metal-containing organic dye. In each case the active layer contains a material which absorbs in the near-UV, visible, or near-infrared region. Oligothiophenes can act as the active layer or the interface to connect the electron donor and the acceptor.

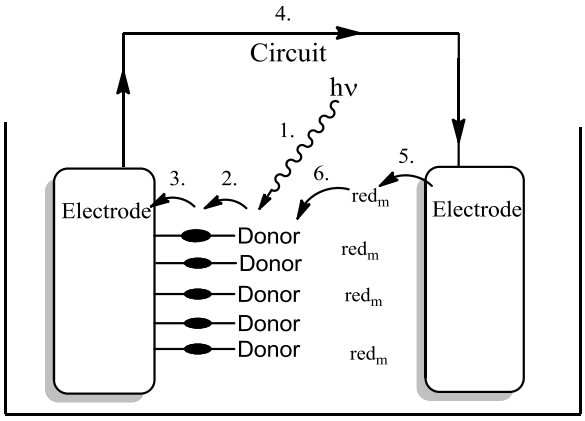

Figure 1.1. Pictorial representation of a generic solar cell. 1. Light creates an exciton in the donor 2. e^- transfer to a charge transfer junction 3. e^- injection into an electrode 4. Current travels through a circuit 5. Spent e^- reduces a redox mediator (red_m) 6. Redox mediator restores ground state donor

The electron acceptor in a solar cell is the electrode connected to a circuit or battery. Before constructing a cell, often a model system is often with an electron acceptor rather than a circuit to show the creation of a free e^- that goes into the electron acceptor. These electron acceptors are electron deficient materials, such as a nanoparticles. Whatever the acceptor is, it often must have a lowest unoccupied molecular orbital (LUMO) lower in energy than the LUMO on the donor from where the e^- originates. The energy of the LUMO of the donor/acceptor

interface, hereafter referred to as charge transfer junction (Figure 1.1), must be between the energies of the LUMO of the acceptor and the LUMO of the donor. One advantage of using oligothiophenes for acceptors is the ease of adjusting LUMOs of oligothiophenes. This can be achieved by extending the chain length, or binding electron withdrawing or donating groups to the thiophene rings. [1-8]

Oligothiophenes are a well-studied class of compounds due primarily to their electronic structure. [9-11] Their highly conjugated electronic structure makes oligothiophenes useful as fluorescent materials in organic light emitting diodes, electron conductors in organic field effect transistors, active phases in organic solar cells, and bridges at electron donor/acceptor interfaces. Organic solar cells, specifically organic photovoltaic devices, often contain electron donor/acceptor interfaces. Poor exciton dissociation and slow charge injection at the donor/acceptor interface have kept organic solar cells from outperforming conventional silicon cells.[2] By inserting a charge transfer junction between the donor and acceptor, the charge injection rate can be increased. This charge transfer junction acts as an electron conduit to separate the exciton into a free charge carrier with the electron hole left behind. Oligothiophenes show promising electron and hole mobilities, both key properties for charge transfer junctions.[1-7]

1.1.1. Oligothiophenes as Charge Transfer Junctions

In work by Yang et al.[3] thiophene rings were used as both electron donor and charge transfer junctions. The donor was three fused thiophene rings and the charge transfer junction was oligothiophene chains of three or four subunits (Figure 1.2). This design is referred to as a "D-B-A" (Donor-Bridge-Acceptor) or "D-π-A" (Donor-conjugated spacer-Acceptor).

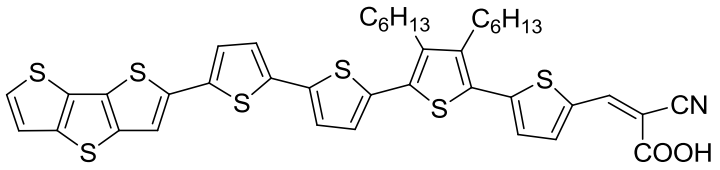

Figure 1.2. Organic dye used for solar cell employing an organic donor (left), oligothiophene charge transfer junction (middle) and a cyanoacrylic acid anchor (right).

Similar work by Choi et al.[4] employed an amine-based organic donor, an oligothiophene chain to support charge transfer and a cyanoacrylic acid functional group which acts as both acceptor and anchoring group for binding to a TiO_2 coated electrode (Figure 1.3). The organic photovoltaic device made from this oligothiophene-containing molecule holds the current record for metal-free organic photovoltaic devices with a power conversion efficiency of 8.60%.[4]

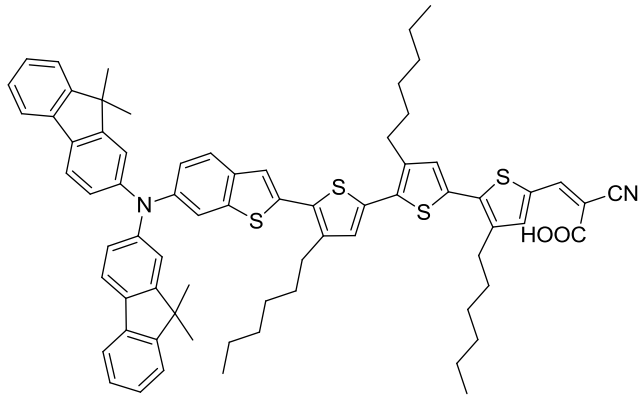

Figure 1.3. Metal-free organic dye composed of an amine donor (left), oligothiophene charge transfer junction (middle) and a cyanoacrylic acid anchor (right).

In the case of metal-free organic dyes, oligothiophene charge transfer junctions can be bound directly to the electron donor. When constructed this way, the oligothiophene chain has the added effect of red shifting the absorbance and increasing the molar extinction coefficient of the dye.[4] Assuming the dye absorbs energy higher than 700 nm, which is virtually always the case, both red-shifted absorbance and an increased molar extinction coefficient are advantageous in organic photovoltaic devices. These effects were demonstrated by the D-π-A compounds of Arakawa et al (Figure 1.4).[5] In their compounds, the peak absorption of the dye was broadened when thiophenes were bound to it, as seen by the absorption of the resulting dyes. The molar extinction coefficient also increased with increasing oligothiophene chain length.

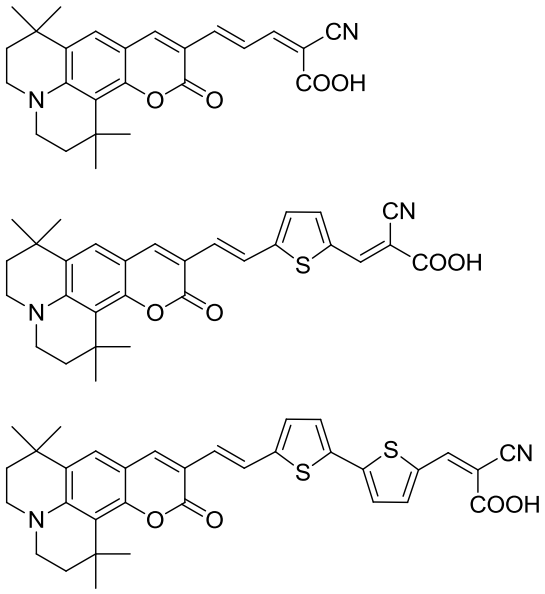

Figure 1.4. Organic dyes that contain D-π-A components. The peak absorption of the initial dye was red-shifted and the molar extinction coefficient increased as a result of binding to thiophenes.

1.1.2. Oligothiophenes Attached to Metal Dyes

Oligothiophene chains can also be electronically connected to metal dyes by being covalently bonded to metal coordinating ligands. Figures 1.5 and 1.6 show several compounds synthesized by the Grätzel[12-14] and Ho[15,16] groups which are examples of metal-containing dyes electronically connected to thiophene moieties.

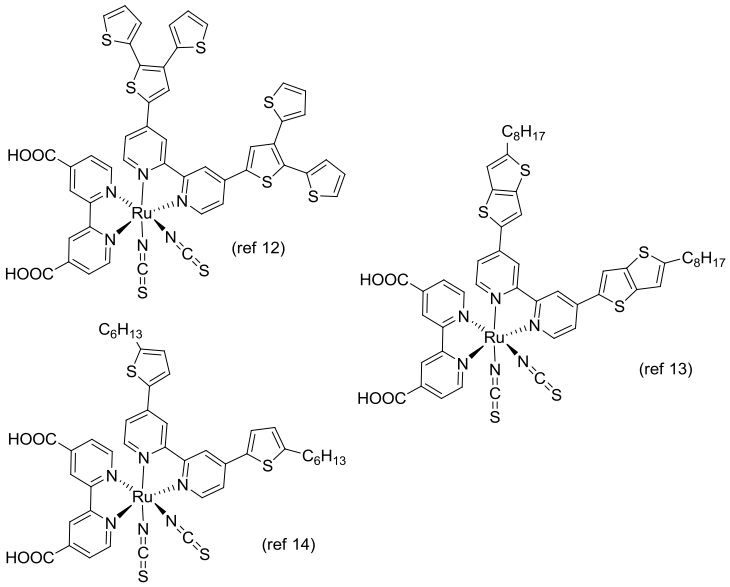

Figure 1.5. Ruthenium dyes bound to thiophenes used by the Grätzel group.

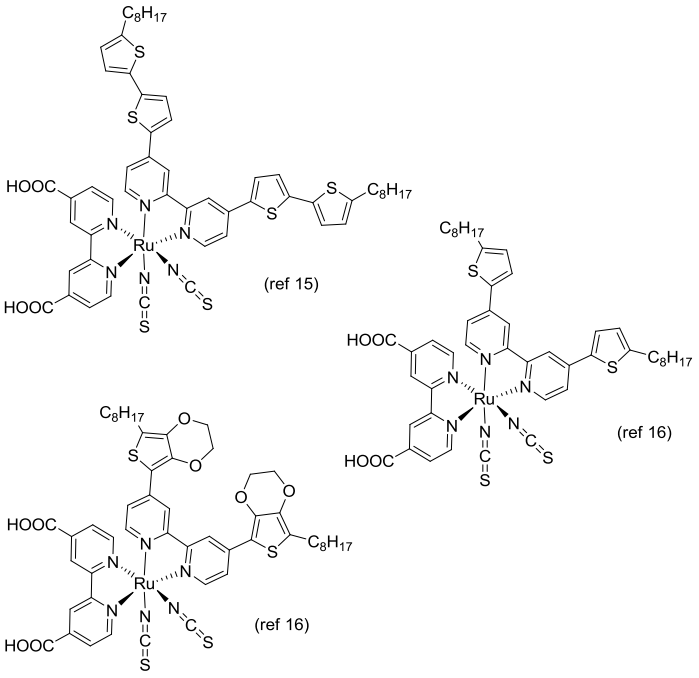

Figure 1.6. Ruthenium dyes bound to thiophenes used by the Ho group.

Houarner-Rassin et al. showed the efficacy of combining Ru dyes with thiophene charge transfer junctions using the compounds shown in Figure 1.7.[18] By including a thiophene ring as a charge transfer junction the number of injected electrons increased by 33%.

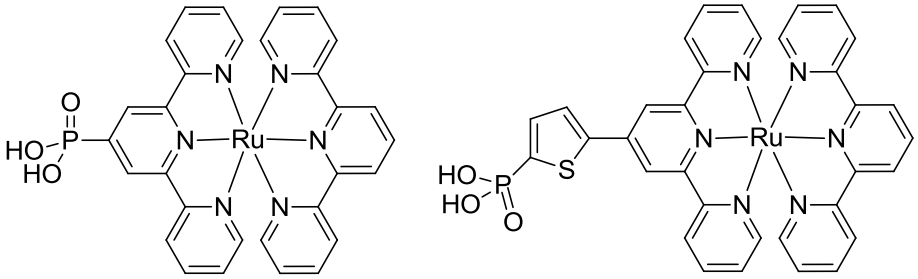

Figure 1.7. Compounds used by Houarner-Rassin et al used a Ru donor and compared with and without a thiophene charge transfer junction.

In work performed previously in our lab, oligothiophene chains were synthesized with bipyridine functional group on one end (Figure 1.8).[17] The bipyridine groups are installed to

chelate with $Ru(bpy)_2^{2+}$, a heavily studied electron donor. By so doing, the oligothiophene is able to act as a charge transfer junction between a Ru dye and an electron acceptor.

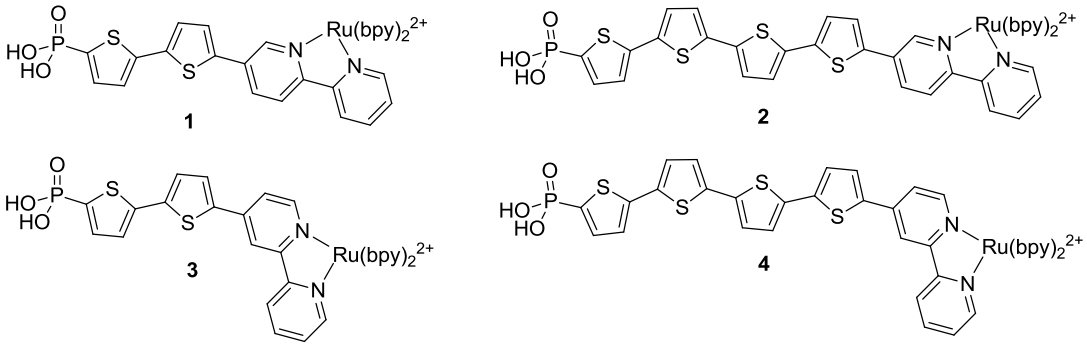

Figure 1.8. Straight chain oligothiophenes bound to $Ru(bpy)_2^{2+}$.[17]

This arrangement of asymmetric oligothiophenes is designed to incorporate an electron donor, Ru(II) along with a charge transfer junction, the oligothiophene, and is prepared to bind a CdSe nanoparticle electron acceptor. This latter binding step will allow preliminary testing on the usefulness of compounds **1-4** in organic photovoltaic devices. The tetramer compounds showed the expected red-shifted absorbance compared to the dimers (Figure 1.9) because of smaller HOMO-LUMO band gaps. Fluorescence measurements of these compounds showed quenching of both the $Ru(bpy)_3^{2+}$ and oligothiophene emission. This result suggests either charge transfer between the thiophene and $Ru(bpy)_2^{2+}$ or the creation of a new vibrational pathway from the excited to ground state.

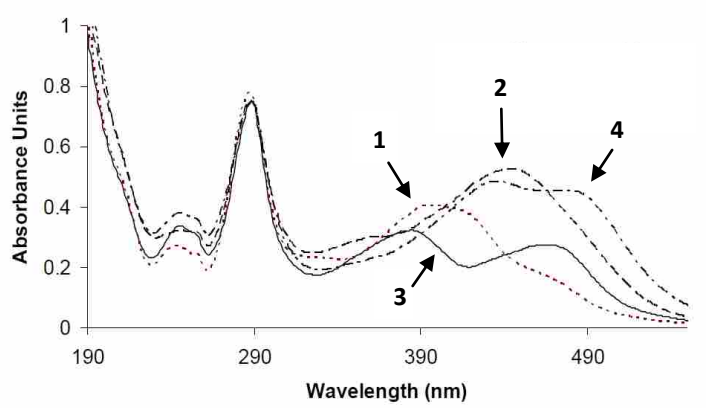

Figure 1.9. Absorbances of compounds **1**-**4.**[17]

1.1.3. Oligothiophene Anchoring Groups

To complete the connection between donor and acceptor, the oligothiophene chain is equipped with an anchoring group to attach to the acceptor. Grätzel, Yang and Arakawa used a cyanoacrylic acid moiety while Hagberg et al. used a cyanoacetic acid moiety.[3-5,19] These choices of anchoring groups work well for binding to TiO_2 surfaces. Along with TiO_2, CdSe nanoparticles are common electron acceptors. Carboxylic acids[20] and phosphonic acids[21] have been frequently used as anchoring groups to CdSe nanoparticles. Of these, the phosphonic acid moiety binds the strongest to CdSe nanoparticles.[21]

Milliron et al.[21] and Locklin et al.[22] bound oligothiophenes to CdSe nanoparticles using a phosphonic acid anchor (Figure 1.10). Both groups were able to bind the oligothiophenes to the nanoparticles under mild heating while stirring overnight under N_2.

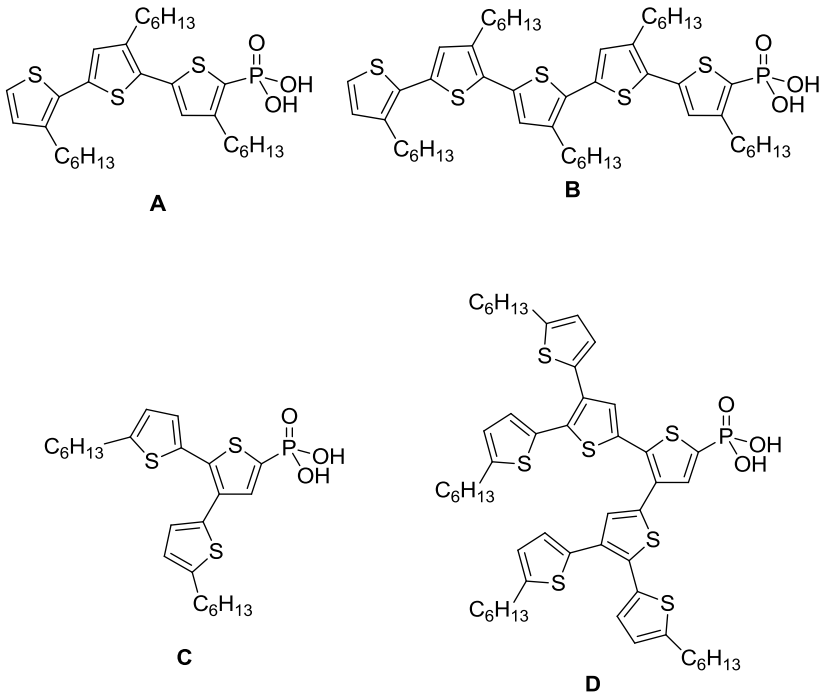

Figure 1.10. Oligothiophenes used by Milliron[21] (**A**,**B**) and Locklin[22] (**C**,**D**) in solar cells using a phosphonic acid anchor.

1.1.4. Oligothiophene Chain Length

It is well known that extending orbital conjugation lowers the band gap energy of a π- π* transition, which results in broader, red-shifted absorbances. Extending the oligothiophene chain length has this same expected effect. In the work by Milliron[21] trithiophene **A** and pentathiophene **B** were synthesized (Figure 1.10). Both compounds were bound to CdSe nanoparticles but caused different optical properties. **B** caused fluorescence quenching of both the oligothiophene and nanoparticle. This is the result of the HOMO and the LUMO of each being staggered. This result is believed by Milliron to indicate an anionic nanoparticle, and a cationic oligothiophene in the excited state (Figure 1.11).

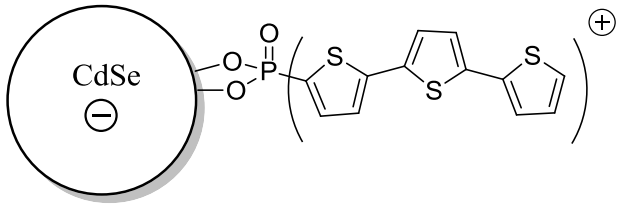

Figure 1.11. Representation of an anionic CdSe nanoparticle and a cationic oligothiophene.

Once this exciton separation happens, neither component is able to fluoresce. When **C** was bound to CdSe nanoparticles the oligothiophene fluorescence was quenched, but the nanoparticle fluorescence increased. This suggests energy transfer from oligothiophene to CdSe nanoparticle, which Milliron takes to mean the CdSe HOMO and LUMO are sandwiched between the HOMO and LUMO of the terthiophene. Milliron proposes that pentathiophenes are the minimum chain length useful in a solar cell, because e^- transfer is needed, not energy transfer.

In contrast, Locklin, while testing dendron oligothiophenes (Figure 1.10, **C** and **D**) showed that charge transfer occurs with **D** as well as **C**, a thiophene with fewer than five subunits.

In an oligothiophene study using an organic dye, Chen et al found an optimal chain length of two thiophenes for their system.[23] In their study they synthesized six different compounds using a tetrahydoquinoline dye, cyanoacrylic anchoring group, and a conjugated spacer in a D-π-A type arrangement (Figure 1.12). As the number of π-bonds increased the absorption band was red-shifted and the molar absorptivity increased. Both of these features are beneficial in an organic photovoltaic device. In conclusion, the optimal oligothiophene chain length depends on the donor and acceptor of the system and supports investigation into the optimal oligothiophene length for any system.

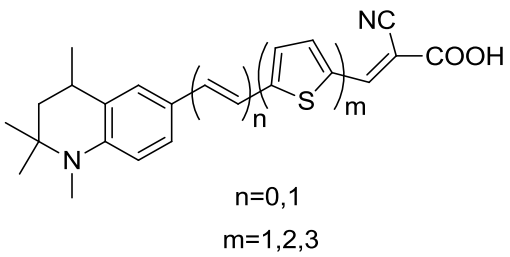

Figure 1.12. Compounds used by Chen et al in a solar cell.

1.1.5. Synthesis of Oligothiophenes

Oligothiophene synthesis has the benefit of being generally predictable because the 2-position undergoes deptotonation and aromatic substitution more readily than the 3-position. Substituent location on oligothiophenes is easily controlled by coupling regioselectively-substituted thiophene subunits.[3,4,24] Aromatic substitution occurs preferentially at the 2-position of thiophene rings as seen in bromination of thiophene with N-bromosuccinimide (NBS), stannylation, borylation and lithium-halogen exchanges. The less common substitution at the 3-position is carried out by ring closure of an appropriately substituted aliphatic thiol,[22,25] or by bromination at the 3-position using Br_2 and Zn in acetic acid.[26]

Coupling of differently substituted thiophene subunits is carried out using Kumada, Stille and Suzuki couplings. Stannylation in a Stille coupling is carried out using a strong base such as *n*-BuLi or LDA. These kinetic bases remove the proton from the 2 position, which is the most acidic. These properties lead to regioregular oligomers with a 2,2´ construction.

A Kumada coupling is a nickel or palladium catalyzed reaction between an aryl halide and the Grignard reagent of an aryl halide. This reaction is a common method for the synthesis of bithiophene. Because the Grignard reagent is strongly basic and commonly nucleophilic, it is not usually used in the presence of base sensitive groups such as esters, nitriles and amides.

A Suzuki reaction is the coupling of an aryl halide with an aryl boronic acid or ester. Although Suzuki reactions have been used with both thiophenes and pyridine rings, thienylboronic esters and acids are often unstable, and the coupling process often affords low yields.

Stille reactions couple trialkylstannylarenes with aryl halides. Trialkylstannylarenes have the benefit of commonly being stable to column chromatography where Kumada couplings never have chromatographable intermediates and Suzuki couplings only sometimes do. On the down side, Stille couplings have intermediates that are toxic and that are malodorous. Overall, the Stille coupling is the preferred method for coupling thiophenes. Compounds **1**-**4** were synthesized using Stille couplings to provide new aryl-aryl bonds.[17]

To complete the series of compounds synthesized previously in our lab, we present the synthesis and NMR, UV-vis and fluorescence characterization of trithiophenes. This complete series of compounds has oligothiophenes of lengths from two to four allowing us to find the optimal number of subunits for correct HOMO/LUMO transition of the charge transfer junction. We hoped to increase light absorptivity of a Ru donor and create more effective light harvesting compounds.

1.2. Results and Discussion

To synthesize the asymmetric oligothiophenes, the oligothiophene was made in two parts and coupled together. One part has the linker and two of the three thiophene rings. The other has the bipyridine group with one thiophene ring. In the 4-position series, the thiophene chain extends off the fourth position of 2,2′-bipyridine (Figure 1.13).

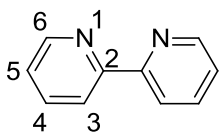

Figure 1.13. Numbering pattern of bipyridine

In the 5-position series the thiophene chain is built off the fifth position of 2,2′-bipyridine. The synthesis of both series requires synthesizing diethyl-2,2′-bithien-5-ylphosphonate (Scheme 1.1) which was coupled to complete the thiophene chain and linking unit. Schemes 1.2 and 1.3 show the synthetic routes for the 5-position series.

1.2.1. Phosphate Half

The phosphate half of the thiophene chain is synthesized using Kumada and Stille cross coupling reactions (Scheme 1.1).[17] The process began by synthesizing bithiophene using a standard Kumada coupling. Bithiophene is then deprotonated by *n*-BuLi and reacted with diethylchlorophosphate to make **5** (T_2P). T_2P is then subjected to *n*-BuLi and tributyltin chloride to make Stille reagent **6** ($TinT_2P$), to be used later in coupling with bipyridine.

Scheme 1.1. Synthesis of **6.**[a]

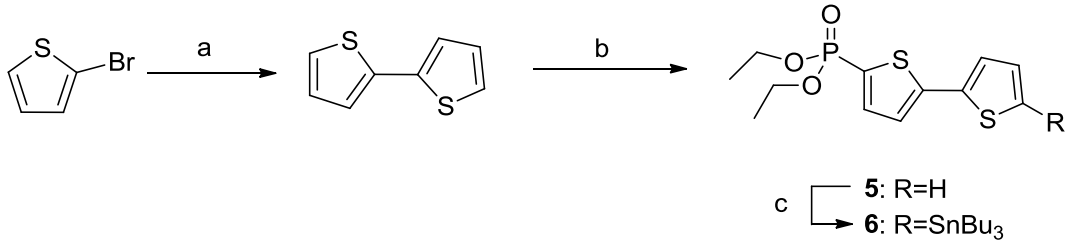

[a]Reagents (a) (1) $Mg_{(0)}$, 60 °C, 15 min; (2) 2-bromothiophene, $Ni(dppp)_2Cl_2$, rt, 16 hr; (b) (1) *n*-BuLi, -78 °C, 1 hr; (2) diethylchlorophosphate, 16 hr; (c) (1) LDA, -78 °C, 1hr; (2) n-Bu_3SnCl, 16 hr.

1.2.2. 5-position trithiophene

Synthesis of the 5-position substituted bipyridines begins with a literature synthesis of **8** (5-Brbpy) (Scheme 1.2).[17] This is done by lithium halogen exchange between *n*-BuLi and 2-bromopyridine to make **7** (tinpyr) and then coupling **7** with 2,5-dibromopyridine under Stille conditions. A Stille coupling of **8** with 2-tributylstannylthiophene afforded **9** (5-Tbpy) in 50% yield (Scheme 1.3). Following the Stille reaction, the product is brominated using NBS to make **10** in 88% yield (5-BrTbpy). Another Stille coupling is performed between **10** and **6** to make diethyl **11** with 53% yield (5-PT_3bpy). Here the ethyl protecting groups are cleaved under neat conditions with TMSBr forming **12** in 89% yield (5-APT_3bpy). The last reaction is ligand exchange with $Rubpy_2Cl_2$ to make **13** with only 5% yield (5-APT-$_3$bpyRu). The low yield is more likely attributed to poor purification than poor yield.

Scheme 1.2. Synthesis of **8.**[a]

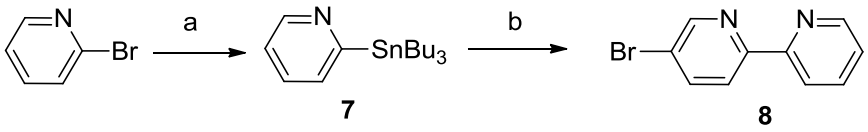

7 **8**

[a]Reagents: (a) (1) *n*-BuLi, -78 °C, 1hr; (2) Sn-*n*-Bu_3Cl, 16 hr; (b) 2,5-dibromopyridine, $Pd(PPh_3)_4$, 120 °C, 72 hr.

Scheme 1.3. Synthesis of **13**.[a]

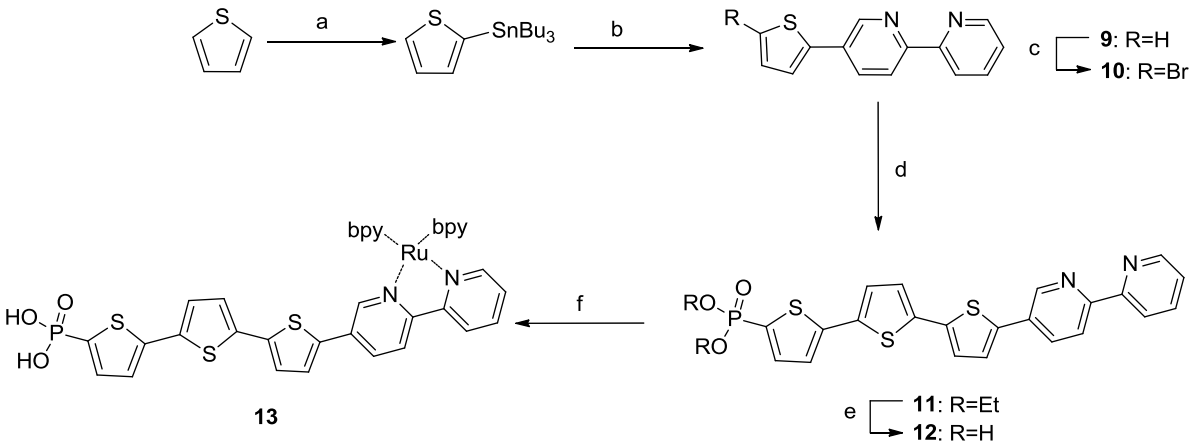

[a]Reagents: (a) (1) *n*-BuLi, -78 °C, 1hr; (2) Sn-*n*-Bu_3Cl, 16hr; (b) **8**, $Pd(PPh_3)_4$, 120 °C, 72 hr; (c) NBS, 1:1 AcOH:$CHCl_3$, 60 °C, 15 min; (d) **6**, $Pd(PPh_3)_4$, 120 °C, 72 hr; (e) TMSBr, neat rt, 16 hr; (f) $Ru(bpy)_2Cl_2$, 100 °C, 4 hr, KPF_6.

1.2.3. 4-Position trithiophene

Synthesis of the 4-position substituted bipyridine began with bromination of the four position on the bipyridine (Scheme 1.4).[17] This is done by oxygenating one nitrogen in bipyridine making **14** (O-bpy), nitrating across the ring to make **15** (O-bpy NO_2), and then swapping the nitro group for a bromine via a Sandmeyer reaction to make **16** (4-Brbpy).

Scheme 1.4. Synthesis of **16.**[a]

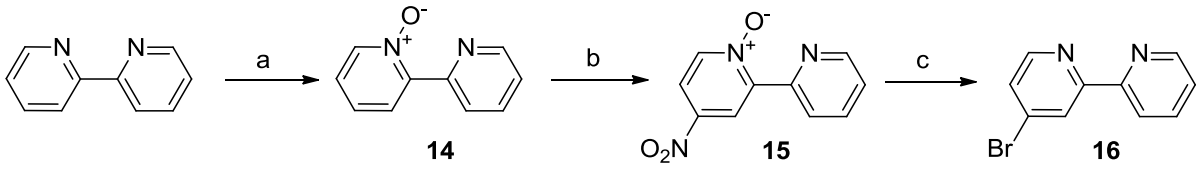

[a]Reagents: (a) MMPP, 80 °C, 4 hr; (b) con. H_2SO_4/HNO_3, 100 °C, 16 hr; (c) (1) Acetyl bromide, 30 °C, 30 min; (2) PBr_3, 100 °C, 1.5 hr.

The first novel compound in this series is made by a standard Stille coupling with 2-tributylstannylthiophene to make **17** (4-Tbpy) in 72% yield (Scheme 1.5). This half is then brominated forming **18** in 61% yield (4-BrTbpy) in preparation to couple with **6** leading to product **19** (4-PT_3bpy). After coupling to form **19** the synthesis is planned similar to the 5-position series with a deprotection of **19** to form **20** and complexing **20** to $Ru(bpy)_2$ to make **21**.

Scheme 1.5 Synthesis of **21.**[a]

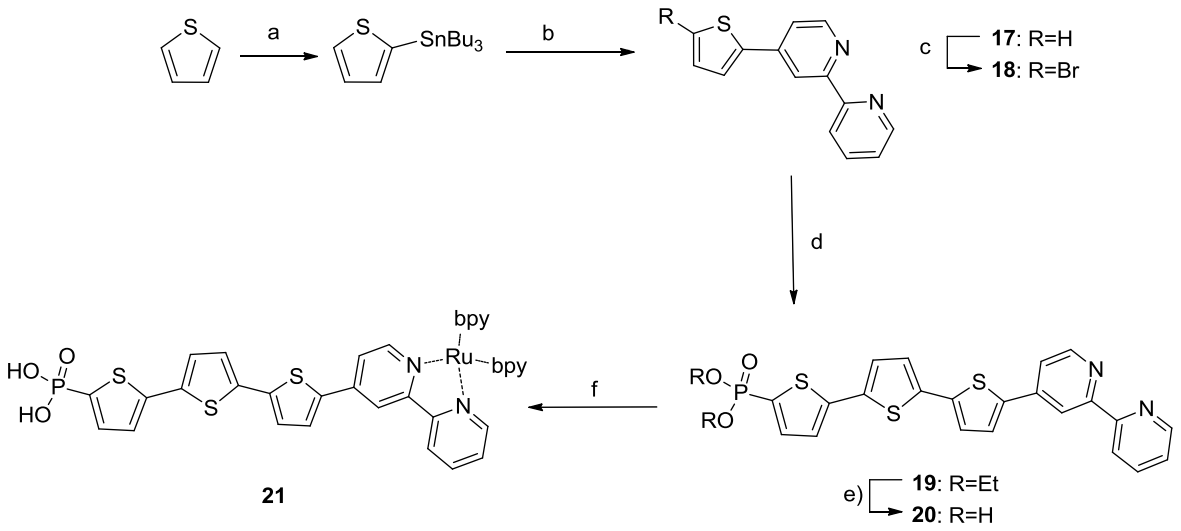

[a]Reagents (a) (1) *n*-BuLi, -78 °C, 1hr; (2) Sn-*n*-Bu_3Cl, 16 hr; (b) **16**, $Pd(PPh_3)_4$, 120 °C, 72 hr; (c) NBS, 1:1 AcOH:$CHCl_3$, 60 °C, 15 min; (d) **6**, $Pd(PPh_3)_4$, 120 °C, 72 hr; (e) TMSBr, neat rt, 16 hr; (f) $Ru(bpy)_2Cl_2$, 100 °C, 4hr, KPF_6.

1.2.4. NMR Assignments

NMR was used throughout the synthesis to identify the product of each reaction. Assigning the NMR spectra of the compounds synthesized required careful and thorough analysis because all of the signals are similar. Thiophene rings are considered to be electron rich and the ^{1}H NMR peaks are found in the upfield limits of the aromatic region. In contrast, pyridine rings are considered electron poor and because of relevant resonance forms, the protons in the 2, 4, and 6 positions are shifted downfield (Figure 1.14). As a result the peaks of compounds **8**, **10**, **11**, **16** and **18** are spread through the aromatic region.[27]

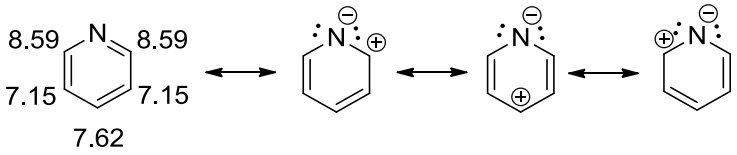

Figure 1.14. Resonance forms that explain the chemical shift pattern of the ^{1}H NMR peaks of pyridine.

To begin the NMR analysis of compounds **8**, **10**, **11**, **16**, and **18**, the peak assignments of simple compounds will be given. As the resonance forms of pyridine show, the 2- and 4-position protons are more electron withdrawn. Replacing a proton in the 2-position with Br makes the 3-position proton appear farther downfield than what is now the 5-position proton. (Figure 1.15).

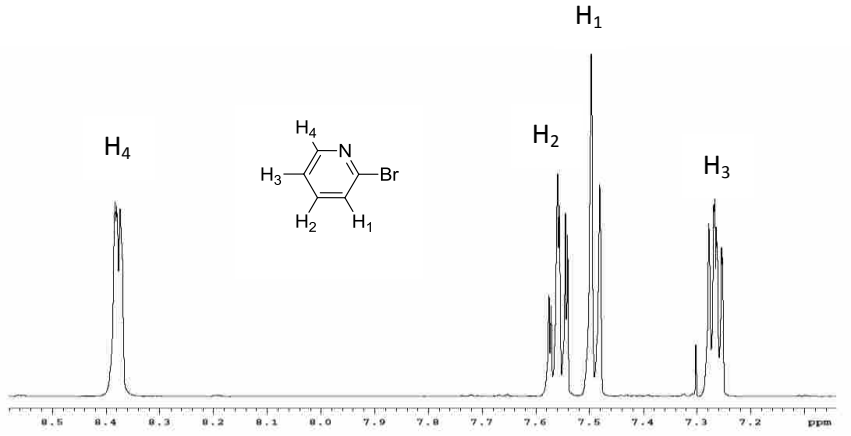

Figure 1.15. ^{1}H NMR of 2-bromopyridine in $CDCl_3$.

Replacing the bromine atom with a bipyridyl group creates symmetry and helps to establish the arrangement of substituted 2,2′-bipyridine groups (Figure 1.16). Resonance forms again explain some of the peak arrangements, with the electronegativity of N and pyridine rings explaining the shifts of the rest. Symmetry makes each peak resemble an identical pair, but each proton is assigned for consistency in discussing the numbering with future structures.

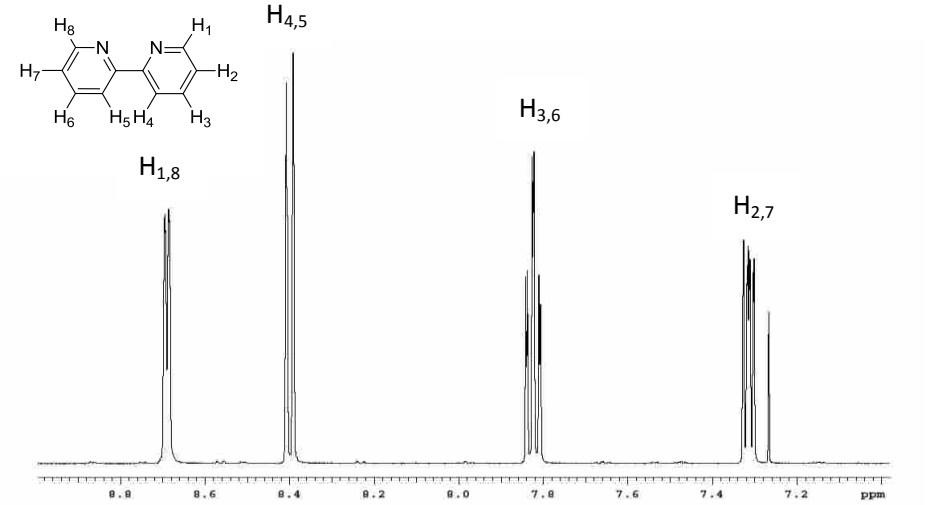

Figure 1.16. ^{1}H NMR of 2,2′-bipyridine.

Using the observations of the previous two compounds we analyze 4-Brbpy (Figure 1.17). 4-Brbpy shows a signal exactly as bipyridine had at approximately 8.7 ppm, which can be

assigned to H_1. The assignment of H_5 can also be based on the downfield shifted position relative to bipyridine owing to the presence of the Br atom, as well as the lack of coupling with the missing H_6, which should be approximately 8 Hz.[27] H_2, H_3, and H_4 remain nearly unaffected. The remaining peak is assigned to H_7, which is appropriately downfield shifted because of the addition of Br. A small amount of O-bpyNO_2 remained.

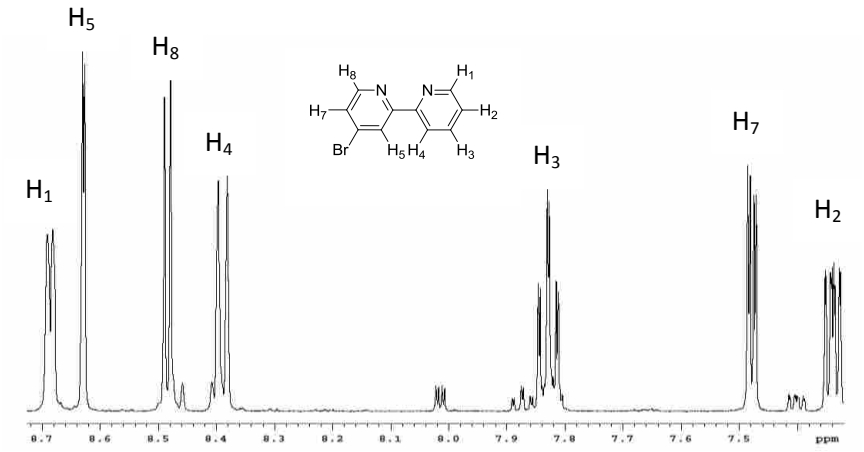

Figure 1.17. ^{1}H NMR of 4-Brbpy (**16**).

The protons affected by the substitution of Br for thiophene, and then bromination of the thiophene are H_5, H_8, and H_7 as seen by slight changes in chemical shift (Figure 1.18).

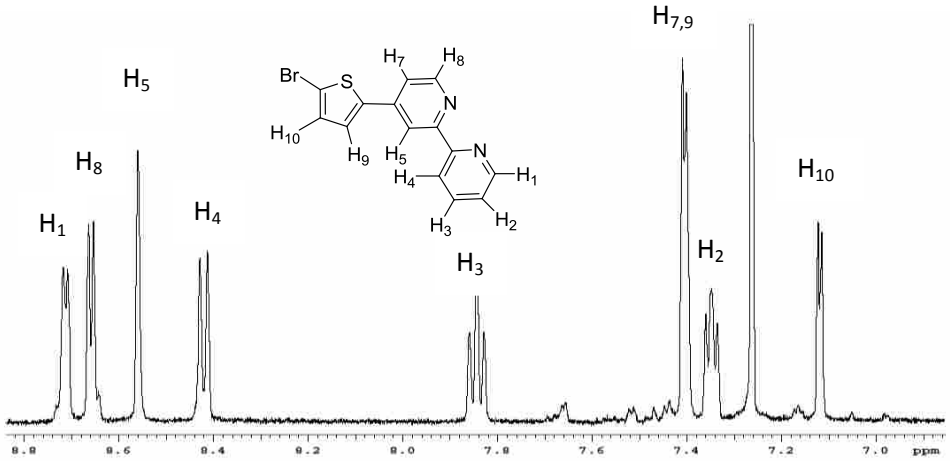

Figure 1.18. ^{1}H NMR of 4-BrTbpy (**18**).

Similarly we can assign the peaks to the 5-position series. 5-Brbpy has peaks similar to 4-Brbpy on the un-substituted ring (Figure 1.19). In contrast to 4-Brbpy, 5-Brbpy peak H_5 retains the splitting with H_6, but H_6 loses its coupling relationship with partner H_7 and is thus no longer a triplet like the analogous 4-Brbpy H_3.

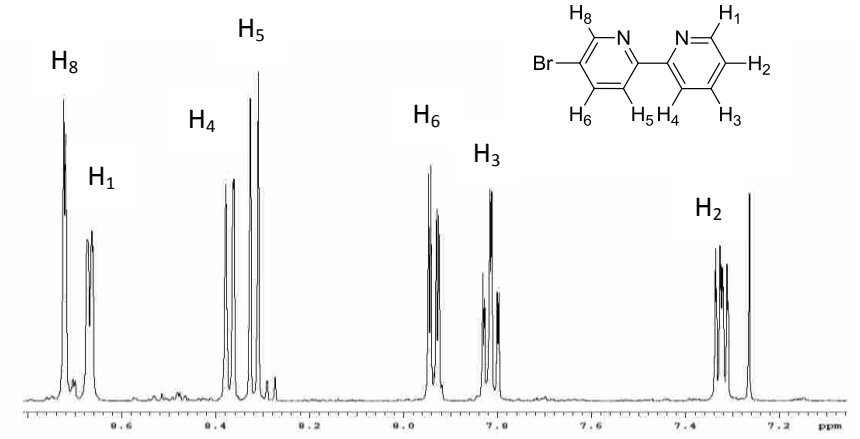

Figure 1.19. ^{1}H NMR of 5-Brbpy (**8**).

5-BrTbpy is similarly arranged, with only a few points to notice (Figure 1.20). First, H_4 and H_5 are not identical, but show accidental chemical overlap, forming a triplet out of two different doublets. It is not a true doublet, however, because the middle peak is not twice the height of the outer peaks, and is in fact broadened due to a slight offset of the two doublets. Furthermore, for unknown reasons, the electronic structure of 5-Tbpy makes the H_9 peak appear significantly shifted compared to that of 4-Tbpy.

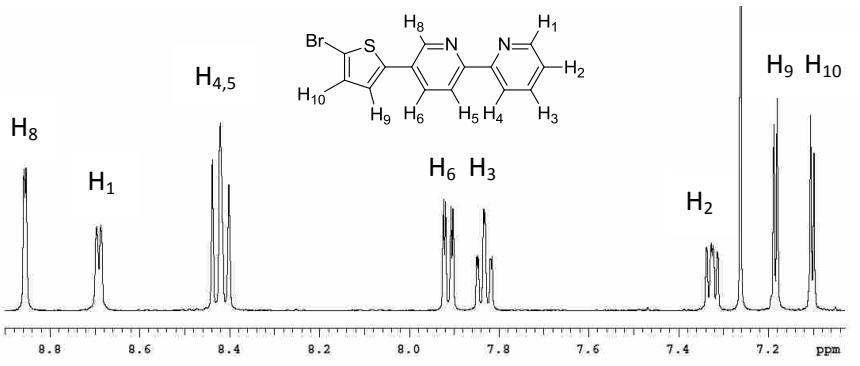

Figure 1.20. ^{1}H NMR of 5-BrTbpy (**10**).

Adding on two more thiophene rings has a significant effect on the chemical shift of H_6, while most of the other peaks remain unaffected (Figure 1.21). The additional thiophene peaks cannot be positively identified in this spectrum.

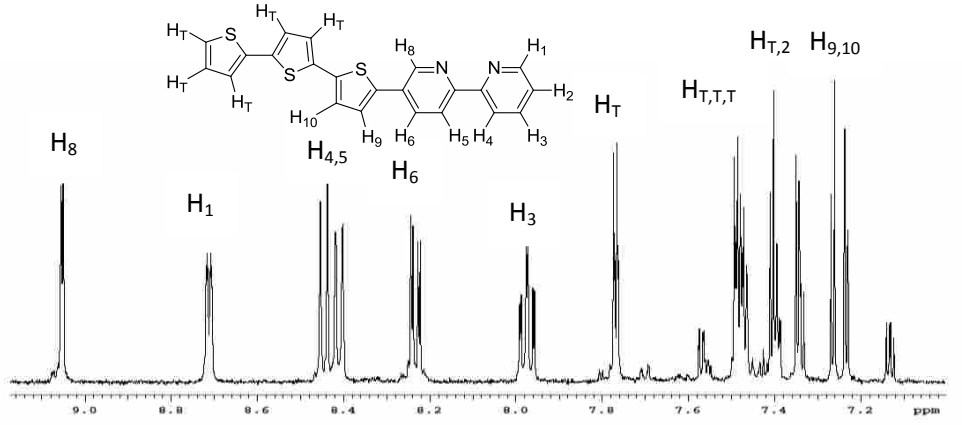

Figure 1.21. ^{1}H NMR of 5-T_3bpy.

Before a discussion of the ^{1}H NMR of 5-PT_3bpy, it will be helpful to understand the coupling partner of 5-BrTbpy: TinT_2P. Here we begin by noting that thiophene peaks are found at 7.30 and 7.10 ppm (Figure 1.22).[27]

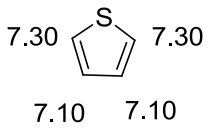

Figure 1.22. Chemical shifts of the ^{1}H NMR peaks of thiophene.[27]

Upon substitution of a proton with another thiophene ring, the ^{1}H NMR of bithiophene was taken (Figure 1.23). H_2 (and equally H_5) shows two different coupling constants with its neighbors leading to a doublet of doublets rather than a triplet.

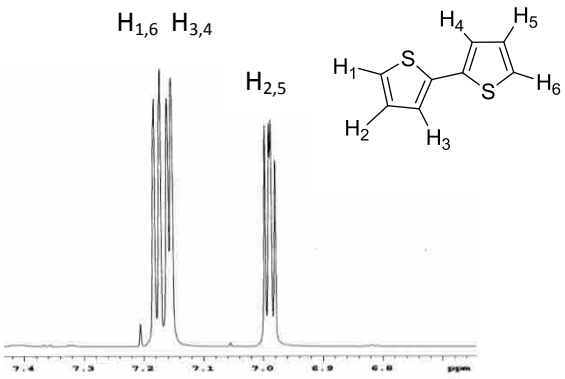

Figure 1.23. ^{1}H NMR of bithiophene.

H_2 again appears similar in TinT, although H_1 is very shifted for unknown reasons (Figure 1.24). The assignment of H_3 is without question, however, because of the satellite peaks created by coupling with Sn. 16.61% of naturally occurring Sn isotopes couple to protons in ^{1}H NMR. Because of this small percentage only small satellite peaks are created.

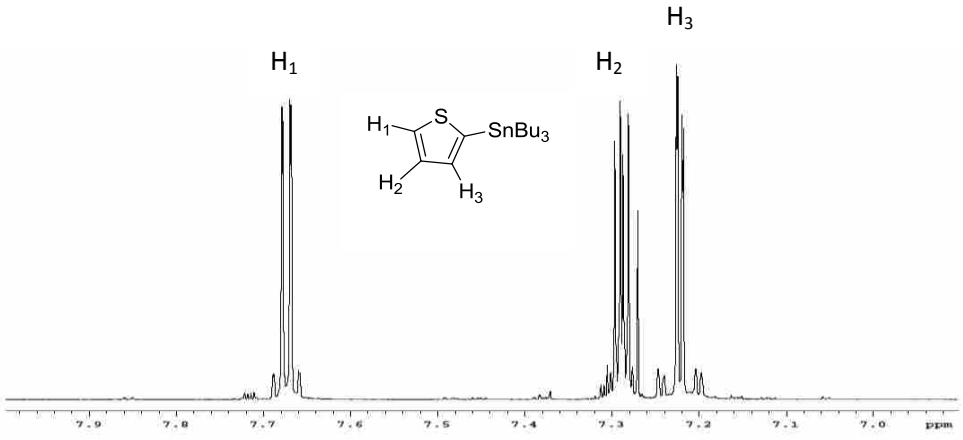

Figure 1.24. ^{1}H NMR of TinT. The tributyl groups are not shown because they are only intermediary and do not help assign peaks in further products.

TinT_2P shows the same Sn satellite peaks which are assigned to H_5, similar to H_3 in TinT (Figure 1.25). H_4 is similar to its counterpart in T_2, but H_2 and H_3 show additional coupling.

This is due to long range coupling with P, which appears in 100% abundance as a spin 1/2 nuclide, giving full splitting in contrast to Sn.

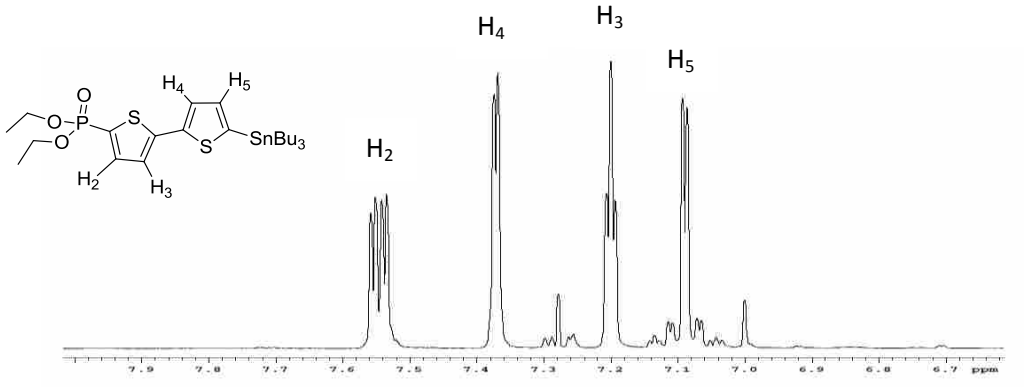

Figure 1.25. ^{1}H NMR of TinT_2P (**6**).

Most of the peaks in 5-PT_3bpy are now ready to be assigned (Figure 1.26). H_1, H_3, H_4, H_5, H_6, and H_8 are similar to 5-T_3bpy and are assigned accordingly. The thiophene peaks are assigned as best as can be determined based on previous compounds.

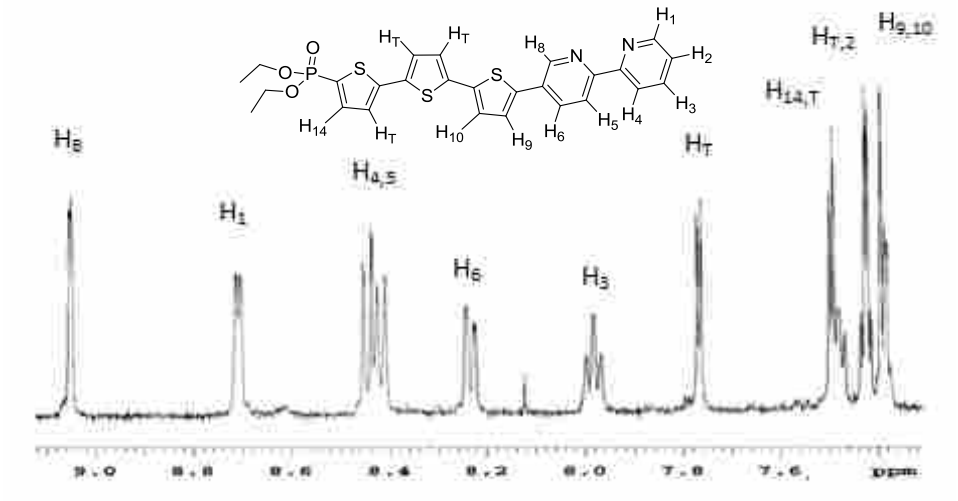

Figure 1.26. ^{1}H NMR of 5-PT_3bpy (**11**).

The final product adds two more bipyridine rings and two phosphonic acid protons. Having three slightly different bipyridine rings makes assigning of individual protons virtually

impossible (Figure 1.27), although assigning a single peak an integral value of 1 shows that the expected 29 protons are present leading us to conclude the compound is 5-APT$_2$bpyRu.

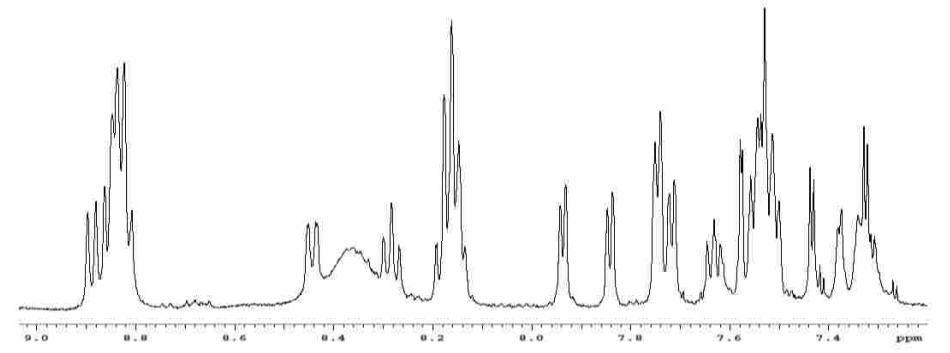

Figure 1.27. ^{1}H NMR of 5-APT$_3$bpyRu (**13**).

1.2.5. Absorbance

An absorbance spectrum of compound **13** was taken and showed similar features to the close analogue, compound **2** (Figure 1.28). The peak at 290 nm is characteristic of the three bipyridine moieties, and the large broad absorption at 450 nm is the result of the π-π* and Ru MLCT transitions overlapping. The molar absorptivity of the 450 nm absorbance is 3 x 10^{-5} M^{-1} cm^{-1}. Compound **13** has an absorption band and molar absorptivity between those of compounds **1** and **2** as expected.

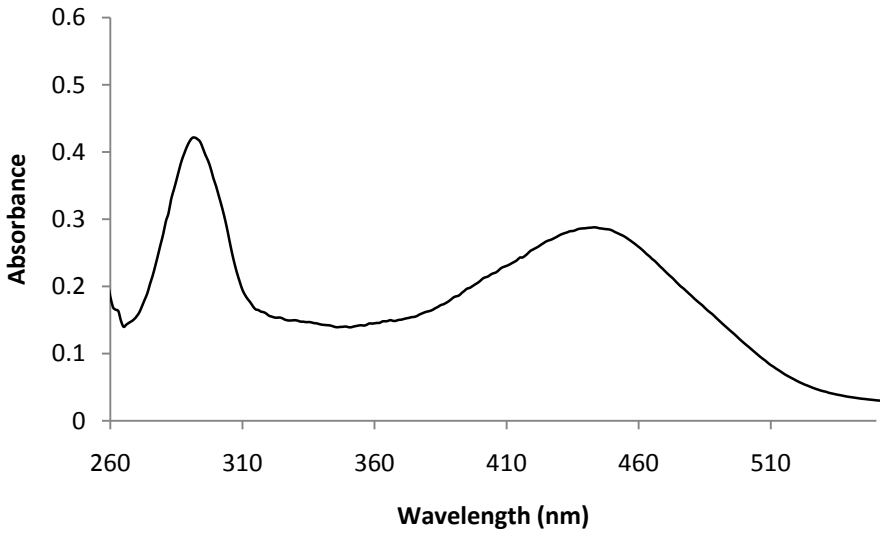

Figure 1.28. Absorbance spectrum of a 0.01 mM DMSO solution of **13**.

1.3 Conclusion

A new bifunctional oligothiophene was prepared and a second is near to completion. The synthetic scheme allows for adjustment of the number of thiophene subunits. NMR spectra have been assigned to support characterization. This synthetic pathway was similar to that used to synthesize four similar oligothiophene compounds with two or four thiophene subunits. The new oligothiophene of three subunits has absorbance features that fit in the pattern of the previously made compounds. These twelve oligothiophenes make a series and are now ready to be bound to CdSe nanoparticles for light harvesting agents.

1.4 Experimental

All starting materials were used as purchased from commercial sources. Dry solvents were obtained from activated alumina columns. Glassware for water-sensitive reactions was oven-dried at 100 °C. N_2 was used as the atmosphere in air-sensitive reactions. Column chromatography was performed using silica gel. All NMR spectra were taken on a 500 MHz

Varian NMR, and referenced to internal TMS. Absorbance measurements were taken on a Hewlett Packard 8453 spectrophotometer.

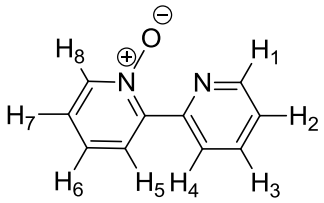

2,2′-bipyridine N-oxide (O-bpy, 14)

Synthesized according to literature procedure.[17] To a 1000-mL flask were added 600 mL ethanol, 2,2′-bipyridine (30.09 g, 193 mmol) and MMPP (35.68 g, 72 mmol). The solution was refluxed for 5 hr and the solvent was removed. 600 mL chloroform were added and stirred for 1 hr. The solid was filtered out through celite, and the solvent was removed. The product was chromatographed using ethyl acetate as eluent, followed by 20% methanol in ethyl acetate. O-bpy (11.75 g, 68 mmol, 47%) was collected as a dark brown oil. ^{1}H NMR ($CDCl_3$, 500 MHz): δ 8.86 (H_8, d, 1H), δ 8.73 (H_1, d, 1H), δ 8.36 (H_4, d, 1H), δ 8.10 (H_5, d, 1H), δ 7.83 (H_3, t, 1H), δ 7.40 (H_6, t, 1H), δ 7.35 (H_7, t, 1H), δ 7.29 (H_2, t, 1H).

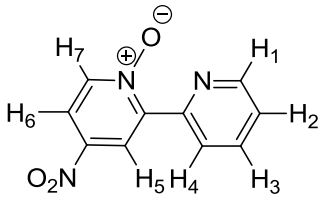

4-nitro-2,2′-bipyridine N-oxide (O-bpy-NO_2, 15)

Synthesized according to literature procedure.[17] Dark brown O-bpy (10.14 g, 59 mmol) was dissolved in 100 mL of conc. H_2SO_4. The solution was brought to 100 °C and 25 mL of conc. HNO_3 were dripped in over a 12 hr period and allowed to react for an additional 3 hrs. The

solution was allowed to cool to room temperature and was then poured into approximately 100 g of ice. $NaOH_{(aq)}$ was added slowly to neutralize the solution, at which point a precipitate formed. The solution and solid were extracted with 100 mL of chloroform and the layers were separated. The aqueous layer was extracted three more times with 100 mL portions of chloroform and the combined organics were washed once with H_2O. The combined organics were dried over $MgSO_4$, filtered through celite, and removed. O-bpy-NO_2 (5.75 g, 28 mmol, 48%) was collected as a pale yellow solid. ^{1}H NMR ($CDCl_3$, 500 MHz): δ 9.16 (H_4, d, 1H), δ 8.90 (H_5, d, 1H), δ 8.80 (H_8, d, 1H), δ 8.36 (H_1, d, 1H), δ 8.07 (H_2, dd, 1H), δ 7.88 (H_6, td, 1H), δ 7.44 (H_7, m, 1H).

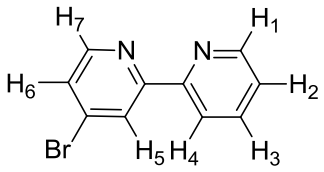

4-bromo-2,2′-bipyridine (4-Brbpy, 16)

Synthesized according to literature procedure.[17] O-bpy-NO_2 (5.57 g, 25.6 mmol) was added to 25 mL glacial acetic acid and heated slightly to dissolve completely. Acetyl bromide (30 mL 405 mmol) was added to the solution and the solution was heated to 30 °C for 30 min. A yellow precipitate formed, but dissolved again upon addition of PBr_3 (21 mL 223 mmol). The solution was heated for 1.5 hrs and then allowed to cool. $NaOH_{(aq)}$ was used to neutralize the solution and extracted with 4 x 50 mL of chloroform. The combined organics were dried over $MgSO_4$, filtered through celite, and condensed to a red oil. 4-Brbpy (4.16 g, 17.7 mmol, 66%) was sublimed from the red oil at approximately 110 °C as a white solid. ^{1}H NMR ($CDCl_3$, 500 MHz): δ 8.69 (H_1, d, 1H, J = 5 Hz) δ 8.61 (H_5, d, 1H, J = 2 Hz) δ 8.49 (H_7, d, 1H, J = 5.5 Hz) δ 8.38 (H_4, d, 1H, J = 8 Hz) δ 7.82 (H_3, td, 1H, J = 2.0, 7.5 Hz) δ 7.48 (H_6, dd, 1H, J = 2, 5.5 Hz), δ 7.34 (H_2, m, 1H).

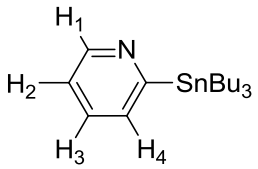

2-tributylstannylpyridine (Tinpyr, 7)

2-bromopyridine (1.2 mL, 12.6 mmol) was added to a dry, N_2 purged Schlenk flask with 40 mL dry toluene and cooled to -78°C. *n*-BuLi (7.9 mL, 12.6 mmol) was added dropwise to the cold solution and allowed to react for 2 hrs. Tributyltin chloride(3.4 mL, 12.5 mmol) was added and the solution was allowed to warm to room temperature overnight. The solvent was removed and about 20 mL hexanes were added and allowed to stir for 45 min. The hexanes were driven off under vacuum and the red-orange oil was chromatographed through silica using 3:1 hexanes:EtOAc. Tinpyr (2.775 g, 7.5 mmol, 60%) was collected as a red oil. ^{1}H NMR ($CDCl_3$, 500 MHz): δ 8.74 (H_1, d, 1H, J = 5 Hz), δ 7.49 (H_2, td, 1H, J = 2, 7.5 Hz), δ 7.40 (H_3, dt, 1H, J = 1.5, 7.5 Hz), δ 7.11 (H_4, ddd, 1H, J = 1.5, 5, 7.75 Hz), δ 1.56 ($SnCH_2\mathit{CH_2}CH_2CH_3$, m, 6H), δ 1.32 ($SnCH_2CH_2\mathit{CH_2}CH_3$, m, 6H), δ 1.12 ($Sn\mathit{CH_2}CH_2CH_2CH_3$, m, 6H), δ 0.88 ($SnCH_2CH_2CH_2\mathit{CH_3}$, t, 9H, J = 7.5 Hz).

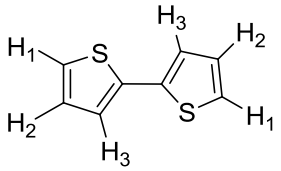

2,2′-bithiophene

Synthesized according to literature procedure.[17] 2-bromothiophene (30 mL, 310 mmol) was added to dry ether with Mg powder (7.30 g, 300 mmol). The reaction was heated until bubbles began forming at which point it was taken from the heat and allowed to reflux from its

own heat for 1 hr. This was cooled in an ice bath and a solution of 2-bromothiophene (30 mL, 310 mmol), $NiCl_2$(dppp) (0.500 g, 0.25 mol%) in dry ether was added via cannula to the reaction. This was allowed to warm overnight and then quenched with 1M HCl. Insoluble salts were filtered out through celite, and the organics were washed with H_2O. The aqueous layer was extracted once with ether and the combined organics were dried over $MgSO_4$, filtered through celite and the solvent was removed. White crystalline bithiophene (9.76 g, 19%) was obtained through sublimation under reduced pressure.

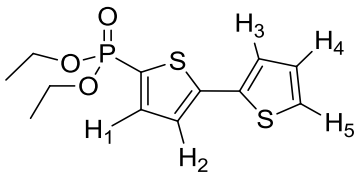

Diethyl 2,2′-bithien-5-ylphosphonate (T_2P, 5)

Synthesized according to literature procedure.[17] Bithiophene (7.903 g, 47.5 mmol) was added to 300 mL of dry THF under N_2 and cooled to -78°C. *n*-BuLi (29.7 mL, 47.5 mmol) was added dropwise and allowed to react for 1 hr. Diethylchlorophosphate (6.9 mL, 47.7 mmol) was added to the solution and allowed to warm to rt overnight. The solvent was removed and the product was dissolved in 100 mL ether and 20 mL H_20. The ether layer was dried over $MgSO_4$, filtered through celite and the solvent was removed. The resulting red-brown oil was chromatographed through silica using 4:1 EtOAC:hexanes. Pure T_2P (12.93 g, 42.8 mmol, 90% yield) was collected as a green oil. ^{1}H NMR ($CDCl_3$, 500 MHz) δ 7.55 (H_1, dd, 1H, *J* = 4, 8.5 Hz), δ 7.25 (H_5, d, 1H, *J* = 5 Hz), δ 7.22 (H_3, d, 1H, *J* = 3.5 Hz), δ 7.16 (H_2, t, 1H, *J* = 3.5 Hz), δ 7.00 (H_4, dd, 1H, *J* = 4, 5.5 Hz), δ 4.11 (O*CH*$_2$CH$_3$, m, 4H), δ 1.31 (OCH$_2$*CH*$_3$, t, 6H, *J* = 6.5 Hz). ESI-TOF $(M+H)^+$ mass: 303.0263.

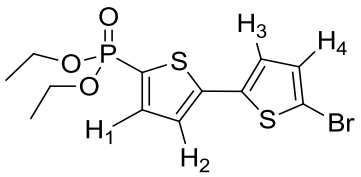

Diethyl 5′-bromo-2,2′-bithien-5-ylphosphonate (BrT_2P)

T_2P (4.80 g, 15.9 mmol) and NBS (2.90 g, 16.3 mmol) were dissolved in 250 mL of 1:1 EtOAC:AcOH. The light yellow solution was heated to 70 °C and left to react for 5 hrs. The orange solution was neutralized with K_2CO_3 and washed with H_2O. The organics were dried over $MgSO_4$, filtered through celite and the solvent was evaporated under vacuum. NMR showed pure BrT_2P in 91% yield (5.49 g, 14.3 mmol). ^1H NMR ($CDCl_3$, 500 MHz): δ 7.52 (H_1, dd, 1H, *J* = 4, 8.5 Hz), δ 7.12 (H_2, t, 1H, *J* = 3.5 Hz), δ 6.99 ($H_{3,4}$, s, 2H) δ 4.14 (OCH_2CH_3, m, 4H), δ 1.34 (OCH_2CH_3, t, 6H, *J* = 7.5 Hz). ESI-TOF $(M+H)^+$ mass: 380.9378.

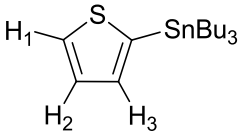

2-tributylstannylthiophene (TinT)

Thiophene (13.5 mL, 169 mmol) was added to a dry, N_2 purged Schlenk flask with 150 mL THF and cooled to -78°C. *n*-BuLi (100 mL, 160 mmol) was added dropwise and the solution was allowed to react for 1 hr under continued cooling. Tri-n-butyltin chloride (43.4 mL, 160 mmol) was added and the solution was allowed to warm to room temperature overnight. The THF was evaporated under vacuum and 75 mL toluene were added. The solution was left to stir for 45 min after which the insoluble salts were filtered out through celite. The toluene was evaporated under vacuum and the resulting pale yellow liquid was chromatographed using

hexanes as eluent. TinT (34.73 g, 93.1 mmol, 58% yield) was collected and is a clear colorless liquid. δ 7.67 (H_1, dd, 1H, J = 1, 5 Hz), δ 7.29 (H_2, dd, 1H, J = 3, 4.5 Hz), δ 7.22 (H_3, dd, 1H, J = 1, 3.3 Hz), δ 1.60 ($SnCH_2\mathit{CH_2}CH_2CH_3$, m, 6H), δ 1.36 ($SnCH_2CH_2\mathit{CH_2}CH_3$, m, 6H), δ 1.13 ($Sn\mathit{CH_2}CH_2CH_2CH_3$, m, 6H), δ 0.92 ($SnCH_2CH_2CH_2\mathit{CH_3}$, t, 9H, J = 7 Hz).

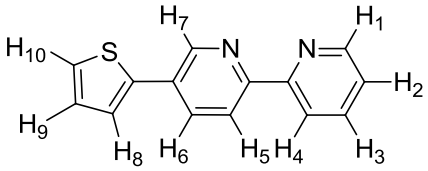

2-(2,2´-bipyridin-5-yl)-thiophene (5-Tbpy, 9)

A 100-mL Schlenk flask was oven dried, purged with N_2 and charged with 50 mL of dry toluene. TinT (5.56g, 14.9 mmol), 5-Brbpy (3.50g, 14.9 mmol) and $Pd(PPh_3)_4$ (0.517 g, 0.45 mmol, 3 mol %) were added to the flask and allowed to reflux for 72 hr. The solvent was removed and the product was dissolved in 250 mL $CHCl_3$ and 50 mL of 2M NaOH. The organics were dried over $MgSO_4$, filtered through celite, and the solvent was removed. The resulting powder was purified through column chromatography using 3:1 ethyl acetate:hexanes. The product was recrystallized in hexanes to yield pure 5-Tbpy in 50% yield. ^{1}H NMR ($CDCl_3$, 500 MHz): δ 8.95 (H_7, d, 1H), δ 8.69 (H_1, d, 1H), δ 8.44 (H_4, d, 1H), δ 8.42 (H_5, d, 1H), δ 8.00 (H_6, dd, 1H), δ 7.83 (H_3, td, 1H), δ 7.44 (H_{10}, d, 1H), δ 7.39 (H_8, d, 1H), δ 7.32 (H_2, m, 1H), δ 7.15 (H_9, t, 1H). ^{13}C NMR ($CDCl_3$, 500 MHz): δ 155.71, 154.85, 149.22, 146.27, 140.42, 136.92, 133.73, 130.29, 128.35, 126.13, 124.32, 123.68, 121.01, 120.98. ESI-TOF $(M+H)^+$ mass: 239.0638.

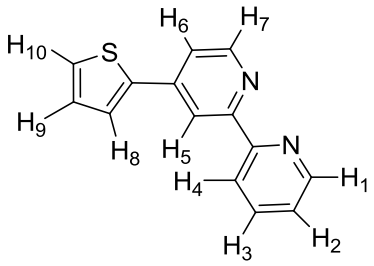

2-(2,2´-bipyridin-4-yl)-thiophene (4-Tbpy, 17)

4-Brbpy (2.32 g, 9.87 mmol), TinT (3.76 g, 10.0 mmol) and $Pd(PPh_3)_4$ (0.93 g, 0.80 mmol, 8.2 mol%) were dissolved in 250 mL of dry toluene under N_2. The solution was brought to reflux for 96 hr. The toluene was then evaporated and the remains were partitioned between 2M NaOH and CH_2Cl_2. The organics were separated off, filtered through celite and the solvent was removed. The remains were subjected to column chromatography using ethyl acetate as eluent followed by 25% methanol in ethyl acetate once the impurities had been removed. 4-Tbpy (1.69 g, 7.11 mmol, 72%) was collected as a yellow brown solid and was without impurities as noted by NMR. ^{1}H NMR ($CDCl_3$, 500 MHz): δ 8.73 (H_1, d, 1H), δ 8.66 (H_7, d, 1H), δ 8.64 (H_5, d, 1H), δ 8.44 (H_4, d, 1H), δ 7.84 (H_3, td, 1H), δ 7.68 (H_{10}, d, 1H), δ 7.51 (H_8, dd, 1H), δ 7.43 (H_6, d, 1H), δ 7.30 (H_2, m, 1H), δ 7.16 (H_9, t, 1H). ESI-TOF $(M+H)^+$ mass: 239.0638.

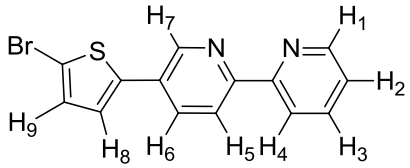

2-bromo-5-(2,2´-bipyridin-5-yl)-thiophene (5-BrTbpy, 10)

5-Tbpy (0.94 g, 3.94 mmol) and NBS (0.71 g, 4.00 mmol) were added to a 500-mL round bottom flask containing 200 mL of 1:1 $CHCl_3$:glacial acetic acid. The mixture was heated for 15

minutes at 60 °C, and allowed to cool. 70 g of NaOH in water was added to the mixture, and the resulting aqueous layer was extracted twice with 50 mL portions of $CHCl_3$. The combined organics were made neutral with K_2CO_3 and then dried over $MgSO_4$. The $MgSO_4$ was filtered out through celite and the $CHCl_3$ was concentrated under vacuum. The resulting solid was washed with 0 °C hexanes. 5-BrTbpy was collected as a yellow solid (1.10 g, 3.46 mmol, 88% yield). ^{1}H NMR ($CDCl_3$, 500 MHz): δ 8.86 (H_7, d, 1H, J = 3.5 Hz), δ 8.70 (H_1, d, 1H, J = 4.5 Hz), δ 8.43 ($H_{4,5}$, t, 2H, J = 9 Hz), δ 7.92 (H_6, dd, 1H, J = 2.5, 8 Hz), δ 7.84 (H_3, td, 1H, J = 1.5, 8 Hz), δ 7.33 (H_2, dd, 1H, J = 5, 7 Hz), δ 7.19 (H_9, d, 1H, J = 4 Hz), δ 7.11 (H_8, d, 1H, J = 4 Hz). ^{13}C NMR ($CDCl_3$, 500 MHz): δ 155.44, 155.08, 149.97, 145.92, 141.85, 137.07, 133.45, 131.18, 129.58, 124.59, 123.85, 121.14, 121.10, 113.01. ESI-TOF $(M+H)^+$ mass: 316.9743.

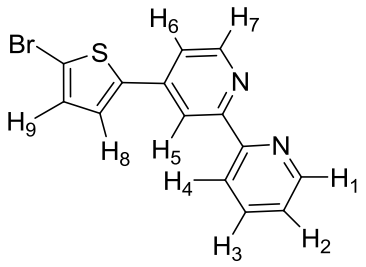

2-bromo-5-(2,2´-bipyridin-4-yl)-thiophene (4-BrTbpy, 18)

4-Tbpy (1.64 g, 6.88 mmol) and NBS (2.58 g, 8.88 mmol) were dissolved in 300 mL of 1:1 $CHCl_3$:AcOH and heated to 60 °C for 30 min. 50 mL of H_2O were added and the layers were separated. The aqueous phase was extracted with 2 x 50 mL of chloroform. The combined organics were neutralized with $K_2CO_{3(aq)}$ and then dried over $MgSO_4$. The solution was filtered through celite and the solvent was evaporated. 4-BrTbpy (1.32 g, 4.16 mmol, 61%) was collected and is clean to NMR. ^{1}H NMR ($CDCl_3$, 500 MHz): δ 8.71 (H_1, d, 1H, J = 4 Hz), δ 8.66 (H_7, d, 1H, J = 5 Hz), δ 8.56 (H_5, d, 1H, J = 1.5 Hz), δ 8.43 (H_4, d, 1H, J = 8.5 Hz), δ 7.84

(H_3, td, 1H, J = 1.5, 8 Hz), δ 7.40 (H_6, d, 1H, J = 3.5 Hz), δ 7.39 (H_8, d, 1H, J = 2 Hz), δ 7.34 (H_2, m, 1H), δ 7.11 (H_9, d, 1H, J = 4 Hz). ^{13}C NMR ($CDCl_3$, 500 MHz): δ 156.82, 155.55, 149.792, 149.14, 142.79, 141.60, 137.05, 131.27, 125.88, 124.04, 121.30, 119.42, 116.83, 114.42. ESI-TOF $(M+H)^+$ mass: 316.9743.

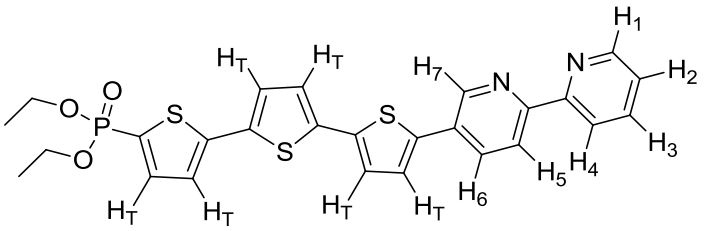

Diethyl 5´´-(2,2´-bipyridin-5-yl)-2,2´-5´,2´´-terthien-5-ylphosphonate (5-PT$_3$bpy, 11)

An oven dried 250-mL Schlenk flask was charged with 100 mL of dry toluene, 5-BrTbpy (0.33 g, 1.0 mmol), TinT_2P (0.61 g, 1.0 mmol), and $Pd(PPh_3)_4$ (0.13 g, 10 mol%) under N_2. The reaction was refluxed for 96 hr. The completed reaction was poured into a 500-mL flask, to which 200 mL of hexanes were added. The resulting precipitate was filtered. 5-PT$_3$bpy (0.29 g, 0.53 mmol, 53% yield) was a red-orange solid. ^{1}H NMR ($CDCl_3$, 500 MHz): δ 9.05 (H_7, d, 1H), δ 8.70 (H_1, d, 1H), δ 8.43 (H_4, d, 1H), δ 8.40 (H_5, d, 1H), δ 8.23 (H_6, dd, 1H), 7.96 (H_3, td, 1H), δ 7.77 (H_T, d, 1H), δ 7.61-7.44 ($H_{2,T,T,T,T,T}$, m, 6H), δ 4.07 (O*C*H_2CH$_3$, m, 4H), δ 1.25 (OCH$_2$*CH*$_3$, t, 6H). ESI-TOF $(M+H)^+$ mass: 539.0685.

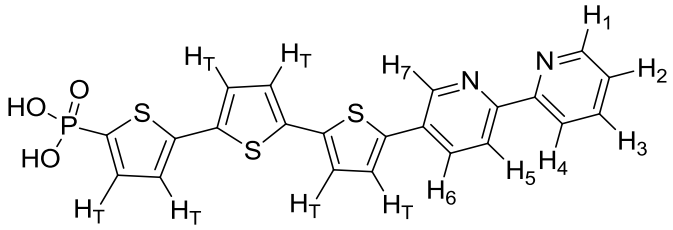

5´´-(2,2´-bipyridin-5-yl)-2,2´-5´,2´´-terthien-5-ylphosphonic acid (5-APT$_3$bpy, 12)

TMSBr (0.6 mL, 4.5 mmol) and 5-PT_3bpy (0.080 g, 0.15 mmol) were added to a dry, N_2 purged Schlenk flask, and the reaction was left to stir overnight under neat conditions. 3 mL $CHCl_3$ and H_2O were added, and the resulting solid was filtered through filter paper and washed with acetonitrile. 5-APT_3bpy was insoluble in common solvents. 5-APT_3bpy was recovered in 89% yield (0.064 g, 0.13 mmol). ^{1}H NMR (DMSO, 500 MHz): δ 9.07 (H_7, d, 1H), δ 8.72 (H_1, d, 1H), δ 8.45 ($H_{4,5}$, t, 2H), δ 8.26 (H_6, dd, 1H), 8.02 (H_3, td, 1H), δ 7.79 (H_T, d, 1H), δ 7.53-7.37 ($H_{2,T,T,T,T,T}$, m, 6H). ESI-TOF (M+H)+ mass: 481.9977.

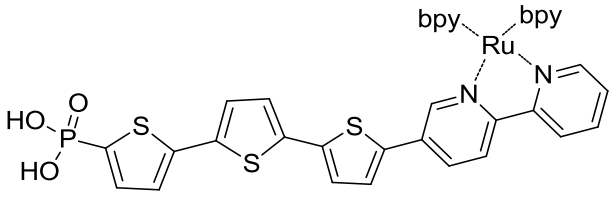

[5´´-(2,2´-bipyridin-5-yl)-2,2´-5´,2´´-terthien-5-ylphosphonic acid]bis(bipyridyl)ruthenium(II) hexafluorophosphate (5-APT_3bpyRu, 13)

5-APT_3bpy (0.1394 g, 0.29 mmol), Ru(bpy)$_2$Cl$_2$ (0.1421 g, 0.29 mmol) and NaOH (0.0171 g, 0.42 mmol) were dissolved in 25 mL H_2O. The solution was refluxed for 4 hr. A solution of KPF_6 (0.3375 g, 1.8 mmol) in 0.3 M HCl was added to the reaction after being allowed to cool. The suspension was centrifuged and the red 5-APT_3bpyRu (0.0168 g, 0.014 mmol, 5%) was collected. ^{1}H NMR (DMSO, 500 MHz): δ 8.92-8.84 (m, 6H), δ 8.47 (d, 1H), δ 8.30 (t, 1H), δ 8.20-8.16 (m, 4H), 7.96 (d, 1H), δ 7.86 (d, 1H), δ 7.76 (d, 2H), δ 7.73 (d, 1H), δ 7.65 (t, 1H), δ 7.60-7.52 (m, 7H), δ 7.47 (d, 1H), δ 7.42 (d, 1H), δ 7.38 (d, 1H), δ 7.37 (d, 1H).

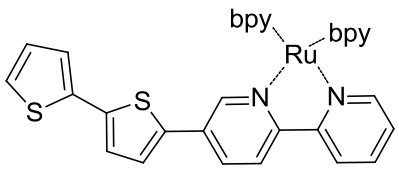

[5′-(2,2′-bipyridin-5-yl)-2,2′-5′,2′′-bithiophene]bis(bipyridyl)ruthenium(II) hexafluorophosphate (5-T_2bpyRu)

5-T_2bpy (0.210 g, 0.66 mmol) and $Ru(bpy)_2Cl_2$ (0.290 g, 0.68 mmol) were dissolved in 30 mL of 190-proof ethanol and refluxed for 6 hr. KPF_6 (1.28 g) in 10 mL H_2O was added and an orange solid precipitated as the solution cooled. The solid was filtered and collected and left to dry under vacuum overnight. Orange-red 5-T_2bpyRu (0.483 g, 0.472 mmol, 72% yield) was clean to ^{1}H NMR. ^{1}H NMR (DMSO, 500 MHz): δ 8.90-8.81 (m, 6H), δ 8.46 (d, 1H), δ 8.28 (t, 1H), δ 8.19-8.15 (m, 4H), 7.95 (d, 1H), δ 7.86 (d, 1H), δ 7.76 (d, 2H), δ 7.73 (d, 1H), δ 7.65-7.52 (m, 8H), δ 7.39 (d, 1H), δ 7.35 (d, 1H), δ 7.15 (t, 1H).

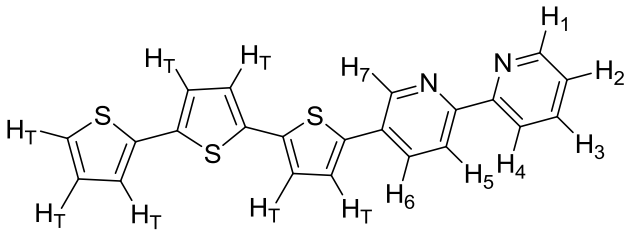

5′′ -(2,2′-bipyridin-5-yl)-2,2′-5′,2′′-terthiophene (5-T_3bpy)

5-BrTbpy (1.1939 g, 3.8 mmol), $TinT_2$ (2.005 g, 4.4 mmol) and $Pd(PPh_3)_4$ (0.6634 g, 0.57 mmol) were dissolved in 125 mL dry toluene in a Schlenk flask. This was connected to a reflux condenser and refluxed for 72 hr. The reaction was cooled, filtered through celite, and the celite was flushed with toluene until the filtrate ran a pale yellow. The toluene was evaporated and replaced with approximately 100 mL of hexanes. The precipitate was filtered through filter paper and retained. The solid was recrystallized in DMSO and then in THF/hexanes producing 5-T_3bpy (0.360 g, 24% yield) as a red solid. ^{1}H NMR (DMSO, 500 MHz): δ 9.05 (H_7, d, 1H), δ 8.72 (H_1, d, 1H), δ 8.45 (H_4, d, 1H), 8.41 (H_5, d, 1H), δ 8.23 (H_6, dd, 1H), 7.97 (H_3, td, 1H), δ

7.76 (H_T, d, 1H), δ 7.49-7.41 ($H_{T,T,T}$, m, 3H), δ 7.39 (H_2, t, 1H), 7.34 (H_T, d, 1H), 7.27 (H_8, d, 1H), 7.24 (H_9, d, 1H). ESI-TOF $(M+H)^+$ mass: 402.0392.

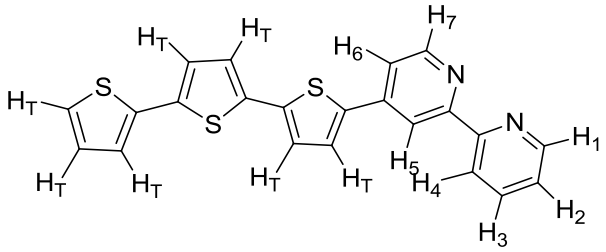

5″-(2,2′-bipyridin-4-yl)-2,2′-5′,2″-terthiophene (4-T_3bpy)

Into 50 mL dry toluene were dissolved 4-BrTbpy (0.1218 g, 0.38 mmol), TinT_2 (0.2142 g, 0.47 mmol) and $Pd(PPh_3)_4$ (0.08 g, 0.07 mmol). The solution was heated to reflux for 72 hr. The reaction was cooled, filtered through celite and the solvent was removed. The toluene was replaced with hexanes and the precipitate was filtered and collected. This solid was recrystallized in DMSO and then in THF/hexanes. 4-T_3bpy (0.158 g, 0.39 mmol, 100%) was a dark red solid. ^{1}H NMR (DMSO, 500 MHz): δ 9.05 (H_1, d, 1H), δ 8.72 (H_7, d, 1H), δ 8.45 (H_4, d, 1H), 8.41 (H_5, d, 1H), δ 8.23 (H_3, dd, 1H), 7.98 (H_6, td, 1H), δ 7.76 (H_T, d, 1H), δ 7.58-7.33 ($H_{2,T,T,T,T,}$ m, 5H), δ 7.13 (H_T, t, 1H). ESI-TOF $(M+H)^+$ mass: 402.0392.

1.5 References

(1) Antoun, T.; Brayner, R.; Al terary, S.; Fiévet, F.; Chehimi, M.; Yassar, A. Facile synthesis of oligothiophene-capped CdS nanoparticles, *Eur. J. Inorg. Chem.* **2007**, *9*, 1275–1284.

(2) Liang, Y,; Peng, B.; Liang, J.; Tao, Z.; Chem, J. Triphenylamine-based dyes bearing functionalized 3,4-propylenedioxythiophene linkers with enhanced performance for dye-sensitized solar cells, *Org. Lett.* **2010**, *12*, 1204–1207.

(3) Yang, H.; Yen, Y.; Hsu, Y.; Chou, H.; Lin, J.; Organic dyes incorporating the dithieno[3,2-*b*:2′,3′ -*d*]thiophene moiety for efficient dye-sensitized solar cells, *Org. Lett.* **2010**, *12*, 16–19.

(4) Choi, H.; Baik, C.; Kang, S.; Ko, J.; Kang, M.; Nazeeruddin, M. K.; Grätzel, M.; Highly efficient and thermally stable organic sensitizers for solvent-free dye-sensitized solar cells, *Angew. Chem. Int. Ed.* **2008**, *47*, 327–330.

(5) Hara, K.; Kurashige, M.; Dan-oh, Y.; Kasada, C.; Shinpo, A.; Suga, S.; Sayama, K.; Arakawa, H.; Design of new coumarin dyes having thiophene moieties for highly efficient organic-dye-sensitized solar cells, *New J. Chem.* **2003**, *27*, 783–785.

(6) Ic, Y.; Hirose, T.; Aso, Y. Synthesis, properties, and FET performance of rectangular oligothiophene, *J. Mater. Chem.* **2009**, *19*, 8169-8175.

(7) Umemoto, Y.; Le, Y.; Saeki, A.; Seki, S.; Tagawa, S.; Aso, Y. Electronegative oligothiophenes fully annelated with hexafluorocyclopentene: synthesis, properties, and intrinsic electron mobility. *Org. Lett.* **2008**, *10*, 1095-1098.

(8) Le, Y.; Umemoto, Y.; Okabe, M.; Kusunoki, T.; Nakayama, K.; Pu, Y.; Kido, J.; Tada, H.; Aso, Y. Electronegative olighiophenes based on difluorodioxocyclopentene-annelated thiophenes: synthesis, properties, and n-type FET performances *Org. Lett.* **2008**, *10* (5), 833–836.

(9) Otsubo, T.; Aso, Y.; Takimiya, K. Functional oligothiophenes as advanced molecular electronic materials, *J. Mater. Chem.* **2002**, *12*, 2565–2575.

(10) Mishra, A.; Ma, C.; Bauerle, P. Functional oligothiophenes: Molecular design for multidimensional nanoarchitectures and their applications, *Chem. Rev.* **2009**, *109*, 1141–1276.

(11) Luo, J.; Qu, H.; Yin, J.; Zhang, X.; Huang, K.; Chi, C. π-Conjugated oligothiophene-anthracene co-oligomers: synthesis, physical properties, and self-assembly, *J. Mater. Chem.* **2009**, *19*, 8202–8211.

(12) Sauvage, F.; Fischer, M., K. R.; Mishra, A.; Zakeeruddin, S. M.; Nazeeruddin, M. K.; Bäurle, Peter; Grätzel, Michael; A dendritic oligothiophene ruthenium sensitizer for stable dye-sensitized solar cells, *Chemsuschem* **2009**, *2*, 761–768.

(13) Gao, F.; Wang, Y.; Zhang, J.; Shi, D.; Wang, M.; Humphry-Baker, R.; Wang, P.; Zakeeruddin, S. M; Grätzel, M.; A new heteroleptic ruthenium sensitizer enhances the absorptivity of mesoporous titania film for a high efficiency dye-sensitized solar cell, *Chem. Commun.* **2008**, 2635–2637.

(14) Gao, F.; Wang, Y.; Shi, D.; Zhang, J.; Wang, M.; Jing, X.; Humphry-Baker, R.; Wang, P.; Zakeeruddin, S. M.; Grätzel, M.; Enhance the optical absorptivity of nanocrystalline

TiO_2 film with high molar extinction coefficient ruthenium sensitizers for high performance dye-sensitized solar cells, *J. Am. Chem. Soc.* **2008**, *130*, 10720–10728.

(15) Chen, C.; Wu, S.; Wu, C.; Chen, J.; Ho, K.; A ruthenium complex with superhigh light-harvesting capacity for dye-sensitized solar cells, *Angew. Chem.* **2006**, *118*, 5954–5957.

(16) Chen, C.; Wu, S.; Li, J.; Wu, C.; Chen, J.; Ho, K.; A new route to enhance the light-harvesting capability of ruthenium complexes for dye-sensitized solar cells, *Adv. Mater.* **2007**, *19*, 3888–3891.

(17) Bair, J. S.; Harrison, R. G. Synthesis and optical properties of bifunctional thiophene molecules coordinated to ruthenium, *J. Org. Chem.* **2007**, *72*, 6653–6661.

(18) Houarner-Rassin, C.; Chaignon, F.; She, C.; Stockwell, D.; Blart, E.; Buvat, P.; Lian, T.; Odobel, F. Synthesis and photoelectrochemical properties of ruthenium bisterpyridine sensitizers functionalized with a thienyl phosphonic acid moiety, *J. Photochem Photobio A* **2007**, *192*, 56–65.

(19) Hagberg, D. P.; Edvinsson, T.; Marinado, T.; Boschloo, G.; Hagfeldt, A.; Sun, L. A novel organic chromophore for dye-sensitized nanostructured solar cells, *Chem. Commun.* **2006**, *21*, 2245–2247.

(20) Fritzinger, B.; Capek, R. K.; Lambert, K.; Martins, J.; Hens, Z. Utilizing self-exchange to address the binding of carboxylic acid ligands to CdSe quantum dots, *J. Am. Chem. Soc.* **2010**, ASAP, DOI: 10.1021/ja104351q.

(21) Milliron, D. J.; Alivisatos, A. P.; Pitois, C. E.; Fréchet, J. M. J. Electroactive surfactant designed to mediate electron transfer between CdSe nanocrystals and organic semiconductors. *Adv. Mater.* **2003**, *15*, 58–61.09

(22) O'Connor, C.; Roydhouse, M.; Przybyl, A.; Wall, M.; Southern, J. Facile Synthesis of 3-nitro-2-substituted thiophenes, *J. Org. Chem.* **2010**, *75*, 2534–2538.

(23) Chen, R.; Yang, X.; Tian, H.; Wang, X.; Hagfeldt, A.; Sun, L. Effect of tetrahydroquinoline dyes structure on the performance of organic dye-sensitized solar cells, *Chem. Mater.* **2007**, *19*, 4007–4015.

(24) Ryu, T. I.; Song, M.; Lee, M. J.; Kang, S.; Lee, J. Y.; Lee, J. W.; Lee, C. W.; Gal, Y. Synthesis and photovoltaic properties of novel ruthenium(II) sensitizers for dye-sensitized solar cell applications, *Bull. Korean Chem. Soc.* **2009**, *30*, 2329–2337.

(25) Afonina, I.; Skabara, P. J.; Vilela, F.; Kanibolotsky, A. L.; Forgie, J. C.; Bansal, A. K.; Turnbull, G. A.; Samuel, I. D. W.; Lambram, J. G.; Anthopoulos, T. D.; Coles, S. J.; Hursthouse, M. B. Synthesis and characterization of new diindenodithienothiophene (DITT) based materials, *J. Mater. Chem.* **2010**, *20*, 1112–1116.

(26) Balaji, G.; Phua, D. I.; Shim, W. L.; Valiyaveettil, S. Synthesis and characterization of unsymmetric indolodithienopyrrole and extended diindolodithienopyrrole, *Org. Lett.* **2010**, *12*, 232–235.

(27) Silverstein, R.; Webser, F.; Kiemle, D.; *Spectrometric Identificiation of Organic Compounds*, 7th ed; Wiley: Hoboken, N.J., 2005

2.1. Introduction

Photovoltaic cells, or more commonly called solar cells, are made up of 4 components: donor, charge transfer junction, circuit, and redox mediator. The sensitizer absorbs the light, the charge transfer junction promotes exciton dissociation and the redox mediator restores the sensitizer ground state. Sensitizers can be organic dyes,[1] organic polymers,[2] inorganic quantum dots,[3,4] metal ion dyes,[5,6] and bulk silicon.[7] Generally, solar cells are categorized as quantum dot solar cells (QDSC) when sensitized by quantum dots, conventional solar cells if made of silicon, or dye-sensitizied solar cells (DSSC) for all other sensitizers. Organic based dye-sensitized cells can be made from cheap and plentiful materials, and have easily tuned absorbances. Despite their potential, they have yet to become common on the market because of their low power conversion efficiencies (PCE). PCE, given the variable η, is the standard measurement of cell efficacy and is calculated according to Equation 1.1 where P is the total power collected by the cell, E is the irradiance striking the cell in W/m^2, and A is the area of the cell in m^2.

$$\eta = \frac{P}{E\ x\ A} x\ 100 \tag{1.1}$$

The highest power conversion efficiency achieved in a dye-sensitized photovoltaic device is barely above 10% by a Ru(II) complex.[8] These metal containing photovoltaic cells currently show the best efficiency, but require costly transition metals. In contrast, quantum dot solar cells (QDSC) generally lack in efficiency, but they are easily tuned. Purely organic dye-sensitized solar cells are made of inexpensive material, but unlike the Ru(II) dyes, have not yet passed 10% PCE.

2.1.1. General Photovoltaic Mechanism

All solar cells follow a general photovoltaic mechanism of exciton formation, exciton dissociation and ground state restoration.[9] An exciton is an excited electron bound to a corresponding electron hole by coulombic attraction. This exciton can be formed in a bulk semiconductor by exciting an electron from the valence band to the conduction band. In a quantum dot or dye-sensitized solar cell, the exciton is formed in the sensitizer when solar radiation excites an electron from the molecule's HOMO to LUMO. This HOMO-LUMO energy difference corresponds to a π to π^* transition in highly conjugated molecules, valence to conduction band transition of quantum dots, or an atomic transition of transition metals. Absorbance measurements with a common UV-vis absorbance spectrometer offer a convenient method to determine the energy gap of a molecule or material.

Exciton dissociation involves separating the excited electron from the corresponding electron hole. The ratio of excitons formed to free charge carriers created is referred to as the internal quantum efficiency. To help in exciton dissociation and increase internal quantum efficiency, a charge transfer junction between electron donor and acceptor is often used. These charge transfer junctions provide a physical pathway for the electron to leave the donor. To do this the transfer junctions must have a LUMO which lies below the energy level of the excited electron to facilitate exciton dissociation. Although absorbance measurements indicate band-gap energies, they do not show the energy levels of the HOMO or LUMO. Cyclic voltammetry can be used for this purpose by measuring the oxidation potential of the HOMO.

Exciton dissociation prevents exciton recombination. Exciton recombination happens when the exciton is allowed to exist long enough for the excited electron to relax into the electron hole and lowers the internal quantum efficiency. This event is accompanied by

vibrational relaxation or by re-emitting the radiation absorbed in the form of light. If steady-state photoluminescent measurements show that a molecule is fluorescent, but that its fluorescence is quenched upon binding a second molecule, then either a new vibrational pathway was created or exciton dissociation was achieved. The work by Milliron et al.[10] illustrates this principle. It was discovered that if an oligothiophene chain was five monomers in length, the HOMO and LUMO of the oligothiophene were above those of the CdSe nanocrystal (Figure 2.1). This HOMO/LUMO arrangement allows for exciton formation into the LUMO of the oligothiophene chain, followed by dissociation into the CdSe nanocrystal LUMO creating an anionic CdSe and a cationic oligothiophene. This is the arrangement that is useful in a photovoltaic device. The excited electron, if not injected into an electrode for use, will relax back to the oligothiophene HOMO through a radiationless relaxation pathway. The net result in this system was quenching of the oligothiophene fluorescence.

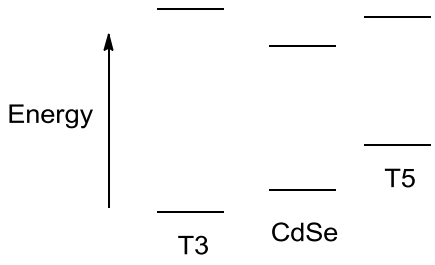

Figure 2.1. Frontier energy levels of CdSe nanoparticles and two oligothiophenes.

When an oligothiophene of three monomer units was used, the HOMO and LUMO of the nanocrystal were between those of the oligothiophene (Figure 2.1). In this case it was claimed that energy transfered from the oligothiophene to the CdSe nanoparticle. This mechanism would include exciton formation in the oligothiophene followed by relaxation of the

exciton, which transfers energy to a CdSe HOMO electron. This new exciton relaxes via a fluorescence pathway. As a result CdSe fluorescence increases and the oligothiophene fluorescence is quenched.

There is another possible explanation for increased CdSe fluorescence. As with the pentamer, the exciton formed in the terthiophene was dissociated into the nanocrystal. In this case, however, an electron in the HOMO of the nanocrystal is able to fall into the HOMO of the oligothiophene chain after excitation, leaving a new exciton in the CdSe nanocrystal. This exciton undergoes recombination and is observed as an increase in the fluorescence of the nanocrystal. If this arrangement does go through a cationic oligothiophene and an anionic nanoparticle, then the process of back electron transfer could compete with dissociation into an electrode, and is therefore not ideal.

2.1.2. Sensitizers

At the heart of any photovoltaic device is the sensitizer. Dye-sensitized solar cells have been studied with Ru,[11] Re,[12] single organic molecule dyes[13] and organic polymers as sensitizers.[14] Quantum dot solar cells have been made using CdS,[15] CdSe[4] and CdTe[16] nanocrystals. Whatever sensitizer is used, it is desired that it has a broad absorption with strong absorption in the red-infrared region. The sun's spectrum as seen at the surface of the earth in the northern hemisphere illustrates why sensitizers need to absorb the near infrared region (Figure 2.2).

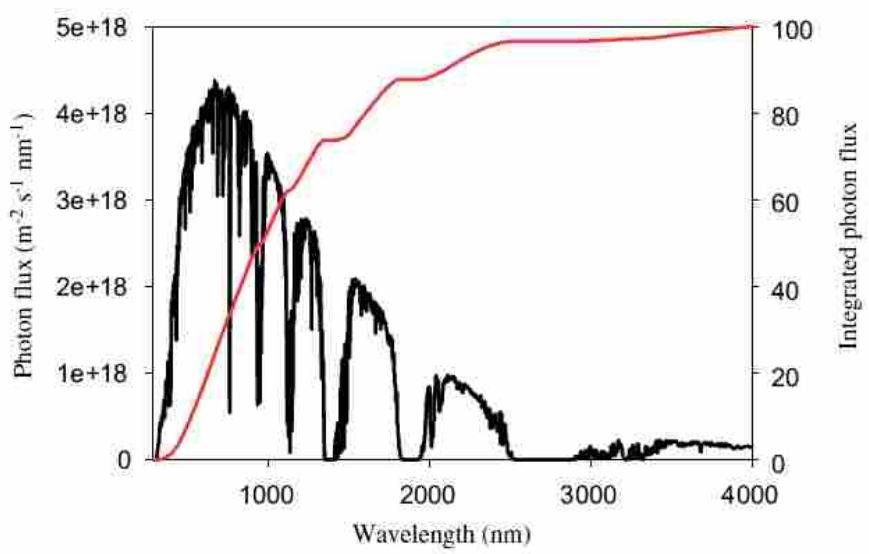

Figure 2.2. Number of photons from the Sun at a given wavelength (black line).[2] The red line is a running integral of all wavelengths starting at 0. Forty-five percent of the available photons from the sun are between the wavelengths of 500 and 1000 nm.

This spectrum is referred to as the AM 1.5 (Air Mass 1.5) spectrum. It represents the irradiance on a square meter surface located at average latitude of the United States and facing normal to the sun when it is 41.81° above the horizon. Fifty three percent of the photons from the sun are found between 280 and 1000 nm and 45% of the photons between 500 and 1000 nm. Because the wavelength of incoming light determines cell voltage, the higher energy photons are the most useful. For these reasons it is generally accepted that the most desirable sensitizers are those that absorb strongly from the near UV to the near infrared.

2.1.2.1. Quantum Dots

Quantum confinement gives QDSC the attractive feature of tuneability. Unfortunately, QDSC are also air sensitive. Debnath et al. theorized two reasons for air sensitivity in QDSC.[17] First, oxidation leads to p-type doping and destruction of the depletion region. Second, oxidation

leads to an increased number of electron traps, which limits the number of free charge carriers acquired at the electrode. To remedy the air sensitivity they reason that a tight binding ligand which doesn't allow oxygen to reach the nanoparticle surface should be used. In addition, this ligand should be strongly conducting to allow charge transport to and from the nanoparticle. They employ *N*-2,4,6-trimethylphenyl-*N*-methyldithiocarbamate as their ligand on PbS nanoparticles. A relatively high efficiency for a QDSC, 3.6%, was reported.

Barea et al.,[18] used CdSe as the sensitizer and TiO_2 nanoparticles as the charge transfer junction on an optically transparent conducting glass electrode. A connecting molecule (mercaptopropionic acid) was used to link the two nanoparticle types together. The carboxylic acid group was bound to the TiO_2 followed by binding of the thiol to CdSe. This gave very poor efficiency and was improved upon by Barea et al.[18] Barea used ZnS to coat the CdSe/TiO_2 nanoparticles to prevent charge recombination with the redox mediator resulting in a PCE of 1.60% under solar irradiation. Mercaptopropionic acid was not used. A further modification on this system by Fan et al was the use of a specialized carbon electrode in place of Pt.[19] Not only was the resulting cell less expensive because of the use of carbon in place of a noble metal, but the resulting efficiency was increased to a record 3.90%.

2.1.2.2. Organic Dyes

Organic dyes have been explored extensively. The advantages of organic dyes are low cost, ease of tunability, solution processing, thinner active layers and production from plentiful starting material. Single molecules and polymers are both used as organic dyes in DSSC.

Single molecule and oligomer organic photovoltaic devices have several advantages over all other such devices. Such compounds have better stability than polymers, cheaper materials

than bulk silicon or transition metal containing devices, currently better efficiency than polymers and QDSC, and cheaper solar cell construction than all other cells.[20] Single organic molecule based cells, with the exception of some non planar structures being currently explored (Figure 2.3), were presented in Chapter 1. Although efficiencies of these and other three dimensional single molecule based solar cells are very modest (PCE of 1%), they are believed to offer better donor/acceptor interfaces.

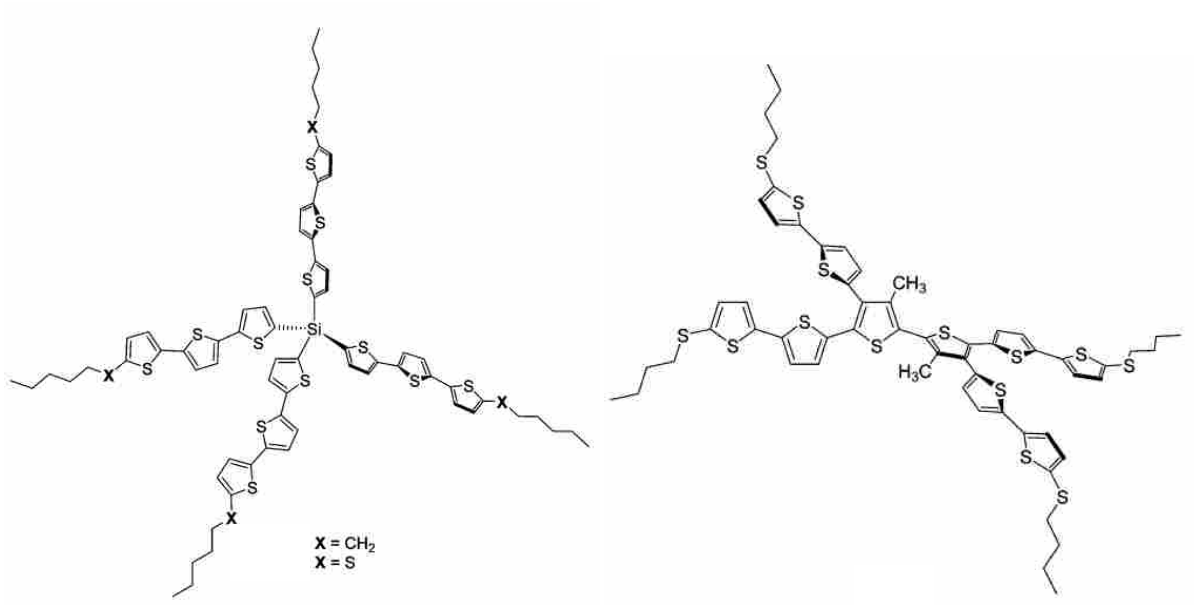

Figure 2.3. Three-dimensional structured molecules for solar cells.

A wide variety of polymers are used in organic photovoltaic devices, including those based on heterocycles that contain sulfur, nitrogen, oxygen, silicon and selenium.[21] Wang et al. used silicon in a polysilafluorene compound (PSiF-DBT, Figure 2.4).[22] In comparison to an analogous compound with carbon in place of silicon (PFDTBT) it was found that the open circuit voltage and closed circuit current of a solar cell was increased with the use of silicon. The voltage change was attributed to the lower HOMO of silicon and the higher current was because of the broader absorption profile. The PSiF-DBT cell showed a high polymer cell PCE of 5.4%.

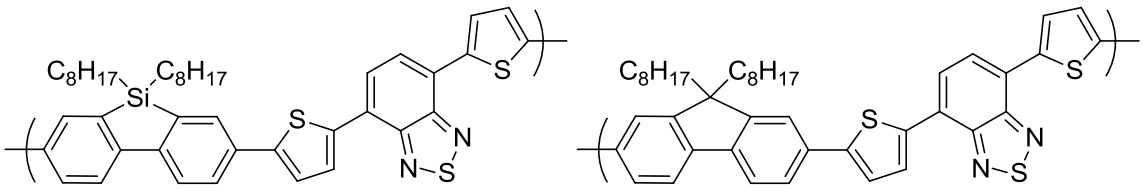

PSiF-DBT PFDTBT

Figure 2.4. PSiF-DBT[22] and PFDTBT[23] polymers used in experimental solar cells. PSiF-DBT showed a better power response than PFDTBT due to the smaller band gap created by the Si atom.

A polymer called PCPDTBT and similar to PFDTBT was used by Peet et al (Figure 2.5).[23] PCPDTBT initially showed only 3.16% PCE,[24] but upon optimization a high PCE of 5.5% was obtained.[23] Hou et al used PSBTBT, a polymer similar to PCPDTBT differing only in the presences of silicone (Figure 6), and saw a decreased average PCE of 4.7%.[25] This PCE was also lower than the similar PSiF-DBT polymer, which contains thiophene rings.

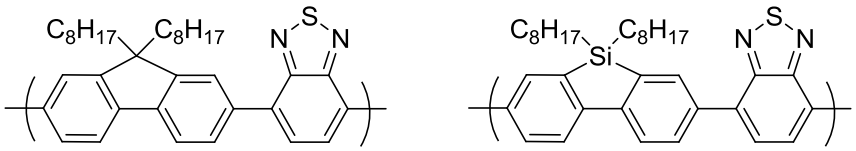

PCPDTBT PSBTBT

Figure 2.5. PCPDTBT[24] and PSBTBT[25] polymers used in a solar cell.

Because of the success of poly-3-hexylthiophene (P3HT), which has been well studied, Liang et al[26] and Wienk et al[27] made P3HT derivatives PTB1 and pBBTDPP2 respectively (Figure 2.6). pBBTDPP2 incorporates an electron poor diketo-pyrrolo-pyrrole moiety with the

purpose of lowering the band gap to harvest the most abundant portion of the solar spectrum. Using this polymer, a PCE of 4% was achieved, which is approximately on par with P3HT efficiencies. Several variations on the diketo-pyrrolo-pyrrole polymer exist, but none have exceeded 4% efficiency.[28,29] PTB1 has a less examined structure, and the beginning stages of research on it have already shown a very promising PCE of 5.6%.

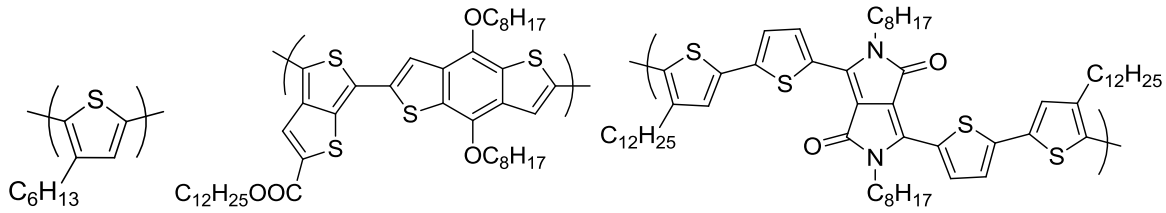

P3HT PTB1 pBBTDPP2

Figure 2.6. PTB1[26] and pBBTDPP2[27] derivatives of P3HT.

2.1.2.3. Metal-containing dyes

Examples of metal-containing dyes include porphyrin analogues[13] and the Ru(II) bipyridyl complexes made by Michael Grätzel.[6] The Ru(II) bipyridyl complex N-719 (Figure 2.7) has shown 11% PCE with an absorption maximum at 530 nm and a nearly quantitative internal quantum efficiency at that wavelength.

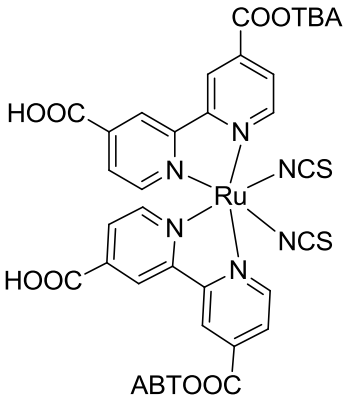

Figure 2.7. N-719 dye made in the Grätzel lab.[6]

The external quantum efficiency, or ratio of free charge carriers to incident photons, at 530 nm was approximately 80%, leaving about 20% loss in efficiency due to absorption and reflection off of the cell structure. At the more desirable 700 nm wavelength, the external quantum efficiency was about 50%. This dye has already begun commercialization after passing a 12,000 h stability test, which exceeds that of amorphous silicon. The most glaring downside of this dye is the incorporation of a rare and expensive transition metal.

Researchers in porphyrin analogs seek to eliminate the need for expensive metals in metal-containing dyes. Most efforts focus on extending conjugation and breaking the symmetry of the porphyrin ring by changing the subsitution on the porphyrin ring to lower the band gap and extend the absorption profile. These principles were used by the Imahori group in the synthesis of Zn-2 (Figure 2.8).[13]

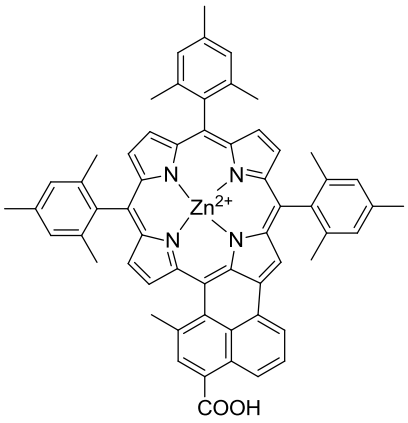

Figure 2.8. Zn-2 dye used in the Imahori group.

The Zn-2 dye is both asymmetric and has mesityl groups to extend the conjugation over a porphyrin ring. The carboxylic acid group is used to bind to the TiO_2 electrode. For the relatively inexpensive Zn-containing porphyrin a PCE of 4.1% was found. This was exceeded by Lee et al. with a Zn-porphyrin that has an electron donating moiety (Figure 2.9), which

extends the absorption profile into the more plentiful part of the solar spectrum.[30] They added several aromatic groups and a binding moiety to various parts of the ring and found the most effective arrangement to be a para relationship between donating and binding groups.[30]

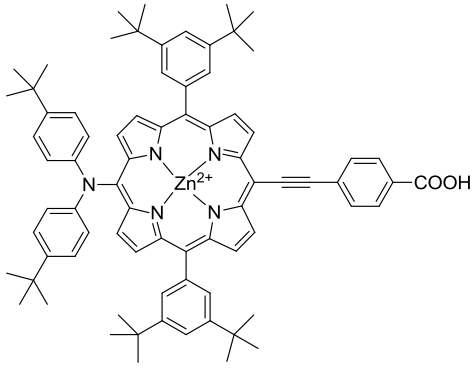

Figure 2.9. Zn-pophyrin ring used by Lee et al. The construction of the dye was designed to extend the absorption into the infrared by addition of an electron rich moiety, extended conjugation through the phenyl rings, and asymmetry overall.

The Grätzel group has also begun work on more inexpensive dyes and made a Zn-porphyrin with an extended unsaturated chain (Figure 2.10). This dye holds the record for PCE of a Zn-porphyrin at 7.1%.[31]

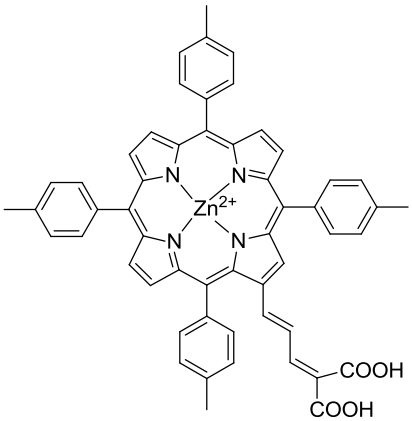

Figure 2.10. Zn-porphyrin dye used in the Grätzel lab with a record 7.1% PCE.

2.1.3. Charge Transfer Junction

Exciton dissociation requires an energy difference for the negatively charged electron to dissociate from the corresponding positively charged hole. That energy, on the order of 0.5 eV, is the minimum difference between the LUMO of the sensitizer and that of the charge transfer junction.[32] If the difference between the LUMO energy levels is less than this threshold, then exciton recombination is favored. If the energy level difference is too large, then the excited electron loses useful energy during exciton dissociation.

A significant obstacle toward high external quantum efficiency is poor free charge carrier creation. The free charge carrier is never created because the exciton recombines before the electron and hole are separated. To solve this problem, researchers have searched for ways to enhance electron and hole mobilities. Currently electron and hole mobilities in organic polymers are limited to 10^{-4} $cm^2/(Vs)$ and 10^{-1} $cm^2/(Vs)$ respectively. Short oligomers such as a hexathiophene used by Aso et al. can achieve better electron mobilities than long ones.[34] Once the exciton reaches the donor-acceptor interface, charge injection can be faster than vibrational relaxation pathways, allowing for so called "hot" electrons (electrons in electronically and vibrationally excited molecules) to enter the conduction band of the acceptor.[9] When this is the case, the limiting factor on how far an exciton can travel before recombination is its mobility getting to the donor-acceptor interface. This limits the exciton diffusion length to approximately 10-20 nm depending on the lifetime of the exciton.[35] In the case of polymer blends this means that for maximum external quantum efficiency, every polymer molecule must be well within 10-20 nm of an acceptor molecule. This fact limits the usefulness of polymer blends because a significant amount of the active layer must be acceptor molecules rather than sensitizers. As polymer electron mobility increases so does the ratio of sensitizer to acceptor that can be used in

an active layer. Increasing the ratio of sensitizer to acceptor increases absorption and free charge carrier creation per unit mass of the cell.

Work by Janssen et al. illustrates these principles.[36] Cells made in their group are a blend of P3HT and ZnO nanoparticles. As the weight % of ZnO increased, the efficiency increased as well. This effect is easily understood as an increase in free charge carrier creation as a result of decreased charge recombination. As the weight % of ZnO increased beyond 26%, however, the efficiency decreased. This is explained by a decrease in the amount of absorbing P3HT as more ZnO is used. Janssen also explains this as formation of ZnO shunts as seen by AFM.

In work performed by Fréchet et al. an amino functionalized P3HT was used to control the dispersion of CdSe nanoparticles.[37] The resulting cell had a maximum efficiency with approximately 40% CdSe by weight. A control P3HT using a non-coordinating Br gave a maximum efficiency at approximately 65 weight % CdSe. The efficiency of the former was greatly increased relative to the latter at their respective maximum efficiencies. This increase in efficiency is likely not a result of a change in hole mobility because the optical spectra were nearly identical between the control and experimental P3HT polymers. Instead, the difference in efficiency is a result of the increased dispersion of CdSe nanoparticles. Increased dispersion results in more free charge carries created per CdSe nanoparticle because there is greater CdSe/P3HT interfacial surface area and less superfluous CdSe.

In a proof of concept by Meyer et al, two charge transfer junctions were used to conduct the hole and excited electron in separate directions (Figure 2.11).[38] In their design phenothiazine is used to resupply the ground state electron to the Ru(II) sensitizer, taking the hole to itself

while the electron passes to a TiO_2 electrode. By physically separating the electron from the hole the lifetime of the charge separated species was increased 1000 fold.

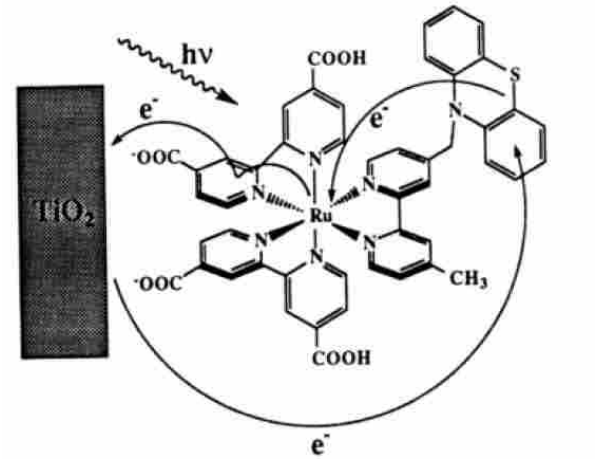

Figure 2.11. Dye used in a DSSC in the Meyer group. An electron is first promoted to the triplet state of the bipyridine, followed by resupplying the ground state by an electron from phenothiazine. The excited electron in bipyridine is then injected into the electrode. The excited electron is used and returned to the ground state of phenothiazine. The result is near elimination of charge recombination at the Ru-bipyridine interface.[38]

2.1.4. Our Photovoltaic System

In this study we use oligothiophene chains as a conjugated system with a low lying LUMO to promote exciton dissociation. We combine a Ru(II) donor and a CdSe nanocrystal acceptor with the oligothiophene charge transfer junction. By varying the properties of the oligothiophene chains, we aim to fine tune the charge transfer junction for a range of sensitizers and acceptors.

2.2. Results and Discussion

Research began on compounds **1** and **2** (Figure 2.12), one from each of the two types of oligothiophenes, those with and without Ru^{2+}.

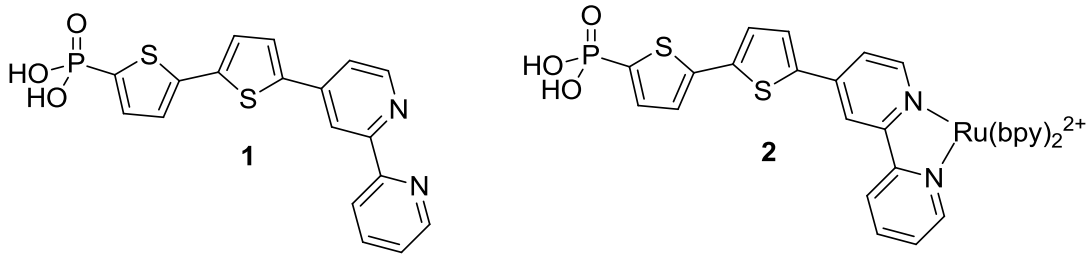

Figure 2.12. Compounds **1** and **2.**

UV-vis absorbance measurements were taken to find the energy gap of the oligothiophenes and nanoparticle before and after binding. Steady-state fluorescence measurements were used to show fluorescence quenching, which is an indicator of efficacy in an organic photovoltaic cell. Time correlated single photon counting was used to find fluorescence lifetimes of CdSe nanoparticles and oligothiophenes before and after binding where possible.

2.2.1. UV-vis Absorbance

The CdSe nanoparticles were with trioctylphosphinoxide (TOPO) ligands and are soluble in nonpolar solvents. UV-vis was used to determine size and concentration of the nanoparticles. CdSe absorption was found to be 547 nm, which corresponds to an average size of 2.97 nm and a molar absorptivity of 1.05×10^5 cm^{-1} M^{-1}. A degassed chloroform solution of CdSe nanoparticles at a concentration of 2.94 μM was prepared for binding to **1** and **2**, which were prepared as degassed butanol solutions. The absorbance spectra for these solutions were taken before mixing (Figures 2.13 and 2.14) and after (Figure 2.15).

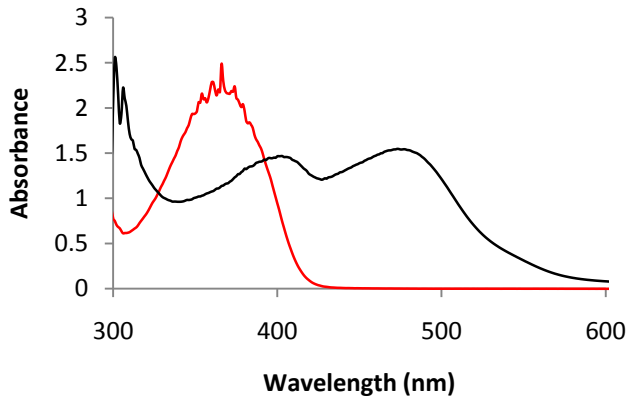

Figure 2.13. Absorbance spectra of butanol solutions of compounds **1** (red) and **2** (black).

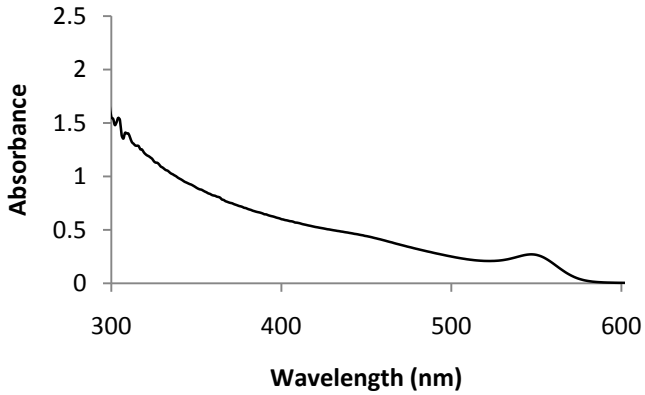

Figure 2.14. Absorbance spectrum of CdSe nanoparticles in chloroform.

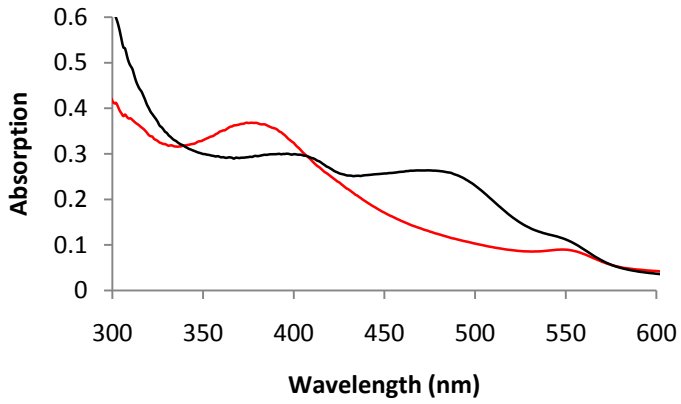

Figure 2.15. Solutions of **1** (red) and **2** (black) each mixed with CdSe nanoparticles.

The absorption at 390 nm for compound **1** is a π-π* transition located in the oligothiophene.[39] Compound **1** shows a similar transition absorbing at 410 nm as well as a Ru MLCT at 540 nm. CdSe nanoparticles show a peak at 550 nm which is a result of the quantum confinement effect and is responsible for the fluorescence emission. All of the known band gap energies and frontier orbital energy levels were calculated using CV and absorbance data as shown above, and are tabulated in Table 2.1.[39]

Table 2.1. Band gap energies and frontier orbital energies of oligothiophenes and 3 nm CdSe nanoparticles.

Compounds	HOMO (eV)	LUMO (eV)	Absorption (eV)	Fluorescence (eV)
4-APT$_2$bpy	1.36	-2.06	3.42	2.85
5-APT$_2$bpy	1.25	-2.04	3.29	2.79
4-APT$_4$bpy	1.15	-1.82	2.87	2.45
5-APT$_4$bpy	1.15	-1.82	2.95	2.55
4-APT$_2$bpyRu	1.4	-1.53	3.23	2.75
5-APT$_2$bpyRu	1.4	-1.43	3.13	2.98
4-APT$_4$bpyRu	1.1	-1.74	2.84	2.55
5-APT$_4$bpyRu	1.1	-1.68	2.78	2.47
CdSe (3 nm)	1.5	-0.69	2.26	2.23

The spectra of the mixtures of oligothiophenes and CdSe are a superposition of the individual absorbances. This suggests that each component maintains its HOMO-LUMO or valence band-conduction band energy gap. Although the oligothiophenes were bound to the nanoparticles, a new molecular orbital did not form as the frontier orbital.

2.2.2. Steady-State Photoluminescence

We used steady-state photoluminescence to investigate the electronic interaction between the oligothiophenes and nanoparticles. 75 μL aliquots of the solution of **2** were added to 1.5 mL of the CdSe solution and the fluorescence of the CdSe was observed after each addition (Figures 2.16). It was found that oligothiphene-ruthenium complex **2** quenches CdSe fluorescence.

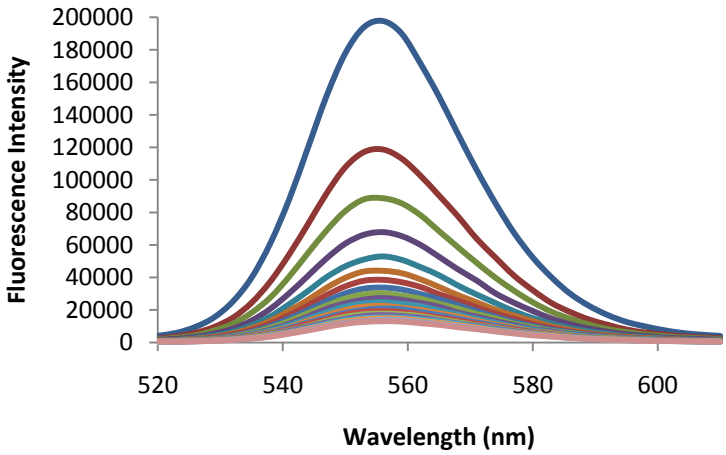

Figure 2.16. Fluorescence measurements of CdSe which decrease with increasing concentration of **1** measured using 350 nm excitation.

The data were compared to equal volume additions of blank solvent and plotted (Figure 2.17) using the Stern-Volmer relationship given in Equation 2 where I_f^0 is the intensity of fluorescence in the absence of quencher, I_f is the fluorescence intensity with quencher, k_q is the quenching constant and C_q is the concentration of quencher.

$$\frac{I_f^0}{I_f} = k_q C_q \quad (2)$$

Each aliquot represents approximately 0.4 equivalents of oligothiophene per nanoparticle. The same data were plotted as a decimal fraction of the fluorescence intensity remaining against the equivalents of oligothiophene added (Figure 2.18). According to the data gathered, 1 equivalent of compound **2** is able to quench 44% of CdSe nanoparticle fluorescence. The remaining fluorescence can be attributed to two possibilities. First it may be that not all of the fluorescence of a nanoparticle is quenched upon binding one oligothiophene. Second, it is alsto possible that not every nanoparticle binds an oligothiophene

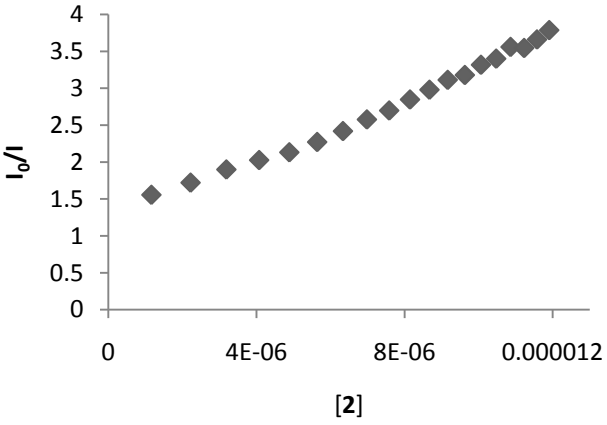

Figure 2.17. Stern-Volmer plot of compound **2** quenching CdSe fluorescence.

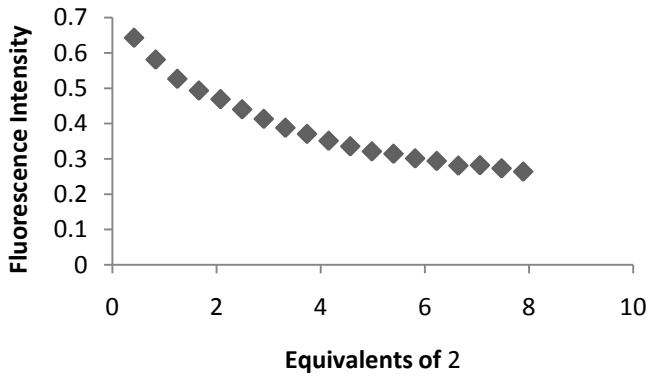

Figure 2.18. Fraction of remaining CdSe nanoparticle fluorescence plotted against equivalents of quencher.

The mechanism for the fluorescence quenching could be a through-space energy transfer, known as a Förster resonance energy transfer (FRET), through bond energy transfer, or electron transfer. To rule out a FRET mechanism from being the mechanism responsible for quenching, an identical experiment was created with an similar compound, but without a phosphonic acid moiety (Figure 2.19). This resulted in precipitation of the CdSe and sporadic data. This is presumably due to the lack of binding oligothiophene which had before bound to the CdSe and kept it in the chloroform/butanol solution. From this we cannot rule out a FRET mechanism as a possible source of fluorescence quenching.

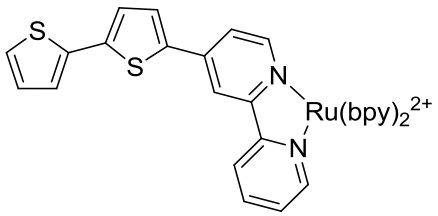

Figure 2.19. Oligothiophene without a phosphonic acid binding group.

A similar experiment was set up using compound **1**. Unlike **2**, **1** does not have a Ru and has a fluorescent emission at 447 nm. This emission overlaps with the emission of CdSe nanoparticles. Figure 2.20 shows a fluorescence spectrum of a 0.9:1 mixture of **1**:CdSe. The emission of **1** was quenched significantly in the presence of CdSe. The effect on CdSe, however, wasn't able to be measured quantitatively because of the significant spectral overlap. Figure 2.21 shows the quantified effects on the fluorescence of **1** by coming in contact with CdSe. More than 95% of the fluorescence of **1** is quenched with 0.2 equivalent of CdSe. This quenching can be explained as each CdSe nanoparticle binding and quenching multiple oligothiophene chains.

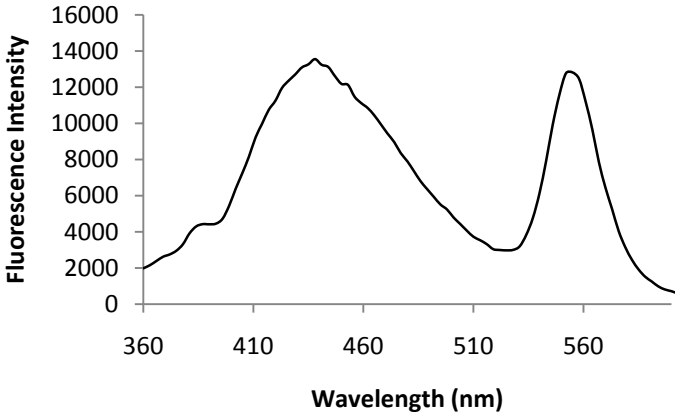

Figure 2.20. Emission spectrum of a 0.9:1 mixture of **1**:CdSe nanoparticles.

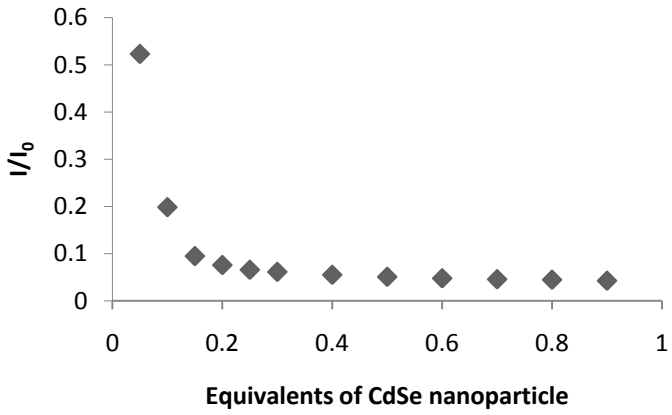

Figure 2.21. Fraction of fluorescence remaining of **1** plotted against equivalents of CdSe nanoparticles.

In a comparison of the 5-position oligothiophenes bound to Ru(II) with two, three and four thiophene subunits (Figure 2.22) it was found that all quenched CdSe nanoparticle fluorescence. Figure 2.23 is an overlay of the data from all three experiments and shows better than 80% quenching of CdSe fluorescence for each.

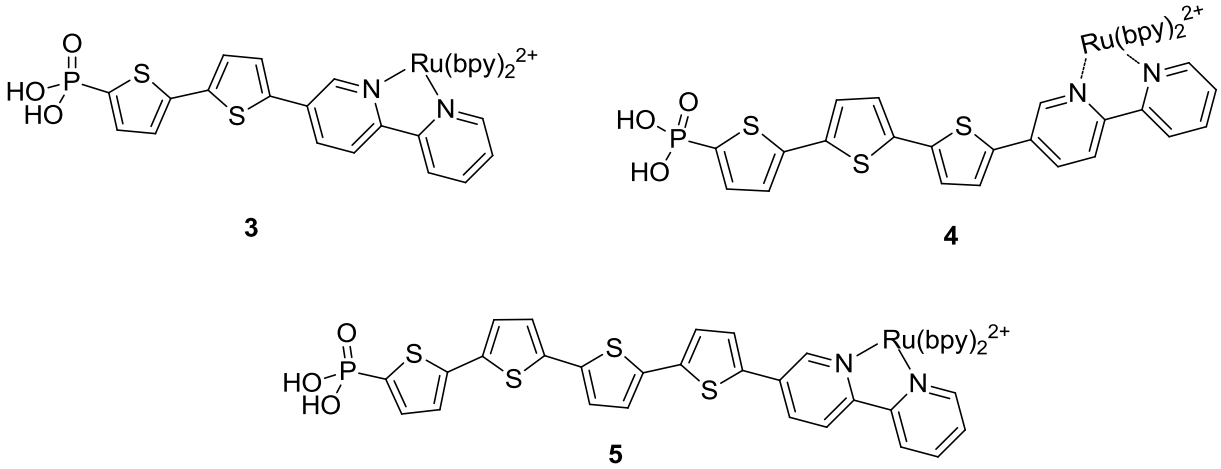

Figure 2.22. Oligothiophenes-ruthenium complexes.

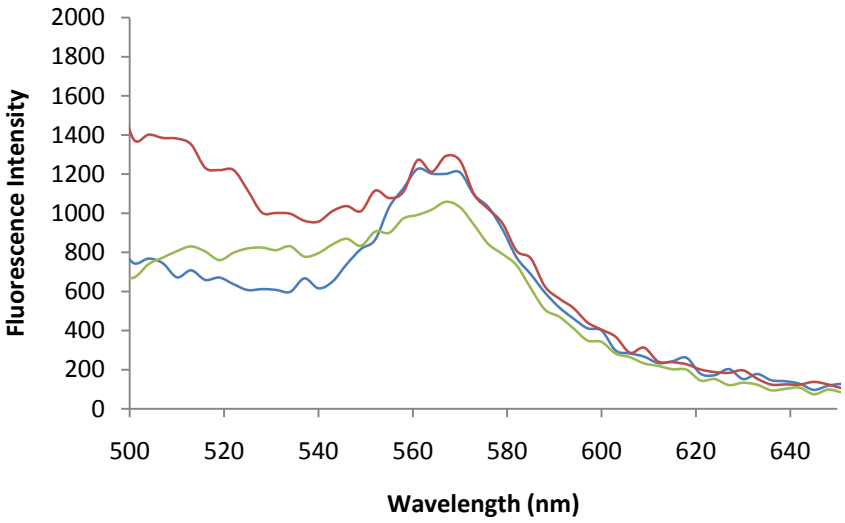

Figure 2.23. Fluorescence quenching of CdSe using compounds **3** (blue), **4** (red) and **5** (green).

2.2.3. Time Correlated Single Photon Counting

Time correlated single photon counting (TCSPC) was used to monitor the fluorescence lifetime of the CdSe nanoparticles used in the fluorescence measurements. The acoustic optical modulator (AOM) used in our experiment was not able to open and close in less than twice the pulse interval of the laser. This lead to a Gaussian buildup and decay of pulses rather than a single laser pulse. The fluorescence lifetime of the CdSe nanoparticles (Figure 2.24) was found to be longer than 12 ns interval between pulses, which lead to a buildup of fluorescence.

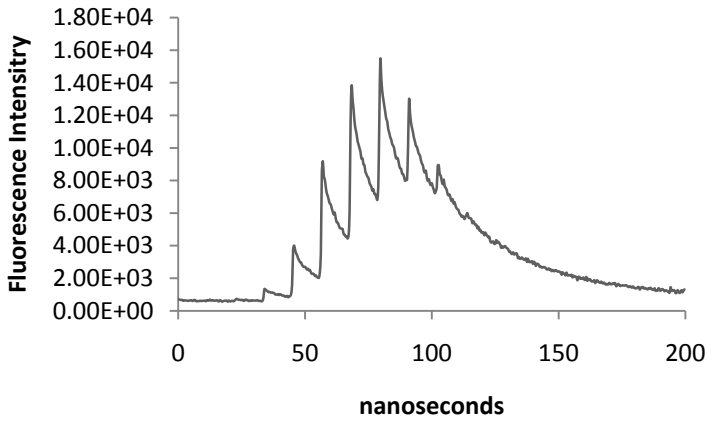

Figure 2.24. Fluorescence lifetime of TOPO capped CdSe nanoparticles in chloroform. Excitation wavelength was 350 nm, fluorescence wavelength was 557 nm.

Upon mixing the CdSe with **2** in a similar manner to the fluorescence experiments, the lifetime data were acquired (Figure 2.25). These data were taken at the same wavelength, 557 nm, and are plotted as a proportion of fluorescence remaining over time. The graph shows a shortened fluorescent lifetime. This is to be expected because the steady-state fluorescence was significantly quenched. Rather than supposing the fluorescence mechanism is faster than before binding the oligothiophene, it is more likely that e^- transfer has become a competitive mechanism to fluorescence. Fluorescent lifetimes of **2** were not measured because the fluorescence was nearly completely quenched.

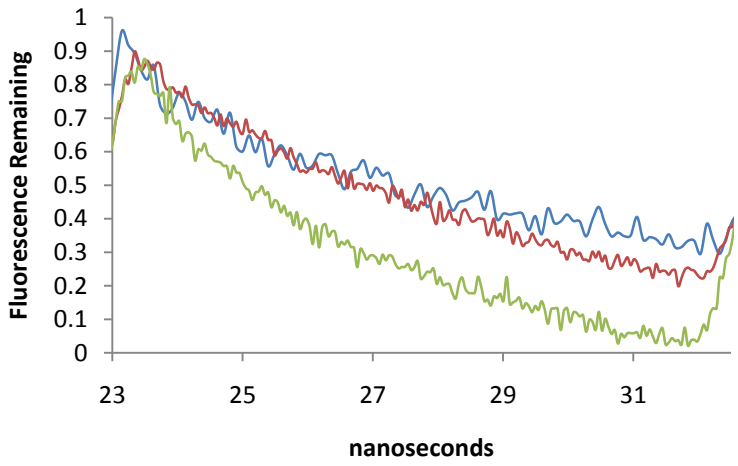

Figure 2.25. Fluorescence lifetimes of CdSe nanoparticles with increasing concentrations of **2** from blue to red to green. Excitation wavelength was 350 nm, fluorescence wavelength was 557 nm.

The fluorescence lifetime of **1** was measured and is given in Figure 2.26. These data show that the fluorescence lifetime of the oligothiophene chain is on the order of a single nanosecond. Because the steady-state fluorescence measurements showed fluorescence quenching of **1** by CdSe nanoparticles, these data suggest that the excited electron transfer from oligothiophene to nanoparticle becomes competitive with fluorescence around the single nanosecond timescale.

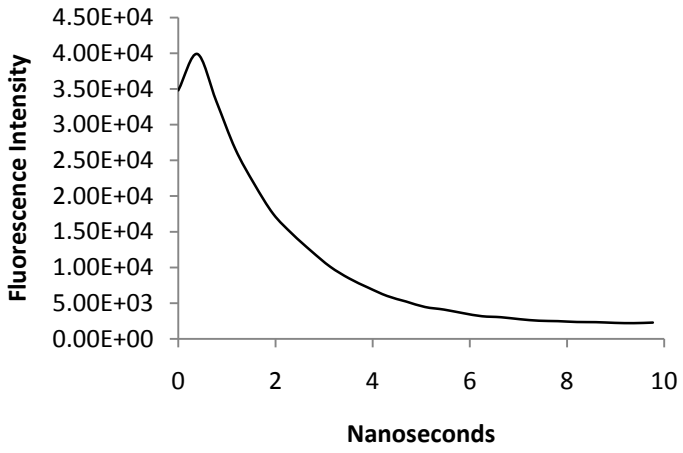

Figure 2.26. Fluorescence lifetime of **1**. Excitation wavelength was 350 nm, fluorescence wavelength was 444 nm.

After binding oligothiophene **1** to CdSe nanoparticles, the data of Figure 2.27 were gathered at 557 nm. These data represent the fluorescence lifetime of the nanoparticle which was previously so long we were unable to see the entire decay before the next pulse from the laser source. This significantly shortened lifetime again suggests a fast electron transfer from oligothiophene to nanoparticle which is on a competitive timescale with fluorescence.

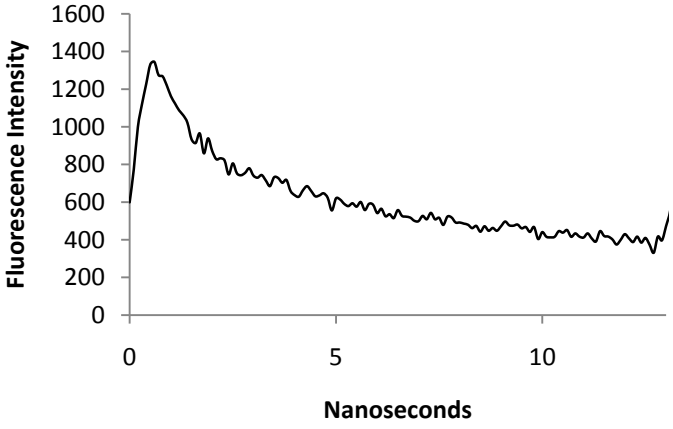

Figure 2.27. Fluorescence lifetime of CdSe nanoparticles bound to **1**. Excitation wavelength was 350 nm, fluorescence wavelength was 557 nm.

2.3 Conclusion

Steady-state fluorescence measurements show that CdSe nanoparticles quench oligothiophenes not bound to Ru. After binding to Ru, the oligothiophene has no fluorescence and quenches that of the nanoparticles. Similar results are obtained regardless of chain length and position on the bipyridine. TCSPC measurements show a decreased fluorescence lifetime of the nanoparticle upon binding with an oligothiophene bound to Ru. An even stronger decrease in fluorescence lifetime is observed when Ru is not present. These preliminary tests suggest electron transfer from oligothiophene to nanoparticle is on the order of single nanoseconds.

2.4 Experimental

Absorbance measurements were made using a glass cuvette on a Hewlett Packard 8453 spectrophotometer in the solvents listed in the text. Steady-state photoluminescence measurements were taken using a quartz cuvette in a Photon Technology International (PTI) Bryte Box fluorometer. Excitation wavelength was set at 350 nm.

Absorbance

All absorbance measurements were taken using a glass absorbance cuvette using the same cuvette with blank solvent to take a background. A new background was taken before each measurement.

Fluorescence

CdSe nanoparticles in TOPO were obtained and melted. 3 mL of melt were dissolved in 15 mL of methanol to dissolve the extra ligand. The suspension was centrifuged and the mother

liquor was discarded. The solid was dissolved in 10 mL $CHCl_3$ and if solid remained it was removed by centrifugation. The solution was diluted until an absorption <1 was found by UV-vis and a concentration could be determined.

All solutions of oligothiophenes and oligothiophene-ruthenium complexes were made by sonicating approximately 50 mg of solid in butanol for 10 min and centrifuged. The saturated solution was retained and the remaining solid was left in the centrifuge tube for future solutions. The solution was diluted until an absorption <1 was found by UV-vis so a concentration could be determined.

All solutions were placed in dry Schlenk flasks equipped with rubber septa and the solutions were degassed by bubbling N_2 through a needle into the solution with the stop cock open. After 15 min the stop cock was closed and the needle removed.

All fluorescence measurements were taken using a step size of 3 nm, using a single integration and no averaging. A quartz cuvette with a rubber septum was used to house the solution.

In quenching experiments, 1.5 mL of the species being quenched was added to an N_2 purged cuvette via syringe, followed by removal of 1 mL of N_2 to maintain pressure. The fluorescence was measured, followed by additions of 75 μL of quenching solution via syringe with readings taken after each addition.

For Stern-Volmer plots the above procedure was followed by an identical blank experiment using 1.5 mL of the species to be quenched with 75 μL additions of degassed solvent identical to that used to dissolve the quenching species.

TCSPC

TSCPC measurements were taken in a quartz fluorescence cuvette using solutions identical to those used in the fluorescence measurements except that they were not degassed. Excitation pulses are from a home built Ti:sapphire femtosecond oscillator which produces 4 nJ pulses at 80 MHz. These were doubled to 400 nm in a Type 1 BBO crystal. The pulse train was chopped by an acusto optic modulator (AOM) to give packets of approximately 8-10 pulses per envelope. Cost limitations led us to use an AOM which was too slow to deliver single pulses. Fluorescence was focused to a quarter meter monochrometer and detected with a photomultiplier tube.

2.5 References

(1) Nelson, J. Organic photovoltaic films, *Curr. Opin. Solid. St. M.* **2002**, *6*, 87–95

(2) Bundgaard, E.; Krebs, F. C. Low band gap polymers for organic photovotaics, *Sol. Energ. Mat. Sol. C.* **2007**, *91*, 954–985

(3) Kamat, P. C.; Quantum dot solar cells, semiconductor nanocrystals as light harvesters, *J. Phys. Chem. C.* **2008**, *112*, 18737–18753.

(4) Mora-Sero, I.; Gimenez, S.; Fabregat-Santiago, F.; Gomez, R.; Shen, Q.; Toyoda, T.; Bisquert, J. Recombination in quantum dot sensitized solar cells, *Acc. Chem. Res.* **2009**, *42*, 1848–1857.

(5) Meyer, G. J. Molecular approaches to solar energy conversion with coordination compounds anchored to semiconductor surfaces *Inorg. Chem.* **2005**, *44*, 6851–6864

(6) Grätzel, M. Solar energy conversion by dye-sensitized photovoltaic cells, *Inorg. Chem.* **2005**, *44*, 6841–6851

(7) Bergmann, R.B. Crystalline Si thin-film solar cells: a review. *Appl. Phys. A: Mater. Sci. Process.* **1999**, *69*, 187-194.

(8) Peter, L. "Sticky electrons" transport and interfacial transfer of electrons in the dye-sensitized solar cell, *Acc. Chem. Res.* **2009**, *42*, 1839–1847.

(9) Brédas, J.; Norton, J. E.; Cornil, J.; Coropceanu, V. Molecular understanding of organic solar cells: the challenges, *Acc. Chem. Res.* **2009**, *42*, 1691–1699

(10) Milliron, D. J.; Alivisatos, A. P.; Pitois. C.; Edder, C.; Fréchet, J. M. J. Electroactive surfactant designed to mediate electron transfer between CdSe nanocrystals and organic semiconductors, *Adv. Mater.*, **2003**, *15*, 58–61.

(11) Grätzel, M. Recent advances in sensitized mesoscopic solar cells, *Acc. Chem. Res.*, **2009**, *42*, 1788–1798.

(12) Walther, M.E.; Wenger, O. S.; *Dalton Trans.* **2008**, 6311–6318

(13) Imahori, H.; Umeyama, T.; Ito, S. Large π-aromatic molecules as potential sensitizers for highly efficient dye-sensitized solar cells, *Acc. Chem. Res.*, **2009**, *42*, 1809–1818.

(14) Brabec, C. J.; Sariciftci, N. S.; Hummelen, J. C. Plastic solar cells, *Adv. Funct. Mater.* **2001**, *11*, 15–26.

(15) Britt, J.; Ferekides, C. Thin-film CdS/CdTe solar cell with 15.8% efficiency, *Appl. Phys. Lett.*, **1993**, *62*, 2851-2852.

(16) Bang, J. H.; Kamat, P. V. Quantum dot sensitized solar cells: A tale of two semiconductor nanocrystals: CdSe and CdTe, *ACS Nano*, **2009**, *3*, 1467-1476.

(17) Debnath, R.; Tang, J.; Barkhouse, D. A.; Wang, X.; Pattentyus-Abraham, A. G.; Brzozowski, L.; Levina, L.; Sargent, E. H. Ambient-processed colloidal quantum dot solar cells via individual pre-encapsulation of nanoparticles, *J. Am. Chem. Soc.* **2010**, *132* 5952–5953.

(18) Barea, E. M.; Shalom, M.; Gimenez, S.; Hod, I.; Mora-Sero, I.; Zaban, A.; Bisquert, J. Design of injection and recombination in quantum dot sensitized solar cells, *J. Am. Chem. Soc.* **2010**, *132*, 6834-6839.

(19) Fan, S.; Gand, B.; Kim, J. H.; Kim, J.; Yu, J.; Ko, J. Hierarchical nanostructured spherical carbon with hollow core/mesoporous shell as a highly efficient counter electrode in CdSe quantum-dot-sensitized solar cells, *Appl. Phys. Lett.* **2010**, *96*, 063501.

(20) Roncali, J. Molecular bulk heterojunctions: an emerging approach to organic solar cells, *Acc. Chem. Res.* **2009**, *42*, 1719–1730.

(21) Chen, J.; Cao, Y. Development of novel conjugated donor polymers for high-efficiency bulk-heterojunction photovoltaic devices, *Acc. Chem. Res.* **2009**, *42*, 1709–1718.

(22) Wang, E.; Wand, L.; Lan, L.; Lio, C.; Zhuang, W.; Peng, J.; Cao, Y. High-performance polymer heterojunction solar cells of a polysilafluorene derivative, *App. Phys. Lett.* **2008**, *92*, 033307–033307-3.

(23) Peet, J.; Kim, J. Y.; Coates, N. E.; Ma, W. L.; Moses, D.; Heeger, A. J.; Bazan, G. C. Efficiency enhancement in low-bandgap polymer solar cells by processing with alkane dithiols, *Nat. Mater.* **2007**, *6*, 497–500.

(24) Muhlbacker, D.; Scharber, M.; Morana, M.; Zhu, Z.; Waller, D.; Guadiana, R.; Brabec, C. High photovoltaic performance of a low-bandgap polymer, *Adv. Mater*, **2006**, *18*, 2884–2889.

(25) Hou, J.; Chen. H.; Zhang, S.; Li, G.; Yang, Y. Synthesis, characterization, and photovoltaic properties of a low band gap polymer based on silole-containing polythiophenes and 2,1,3-benzothiadiazole, *J. Am. Chem. Soc.* **2008**, *130*, 16144–16145.

(26) Liang, Y.; Wu, Y.; Feng, D.; Tsai, S.; Son, H.; Li, G.; Yu, L. Development of new semiconducting polymers for high performance solar cells, *J. Am. Chem. Soc.* **2009**, *131*, 56–57.

(27) Wienk, M. M.; Turbiez, M.; Gilot, J.; Janssen, R. A. J. Narrow-bandgap diketo-pyrrolo-pyrrole polymer solar cells: the effect of processing on the performance, *Adv. Mater.* **2008**, *20*, 2556–2560

(28) Sonar, P.; Ng, G.; Lin, T. T.; Dodabalapur, A.; Chen, Z. Solution processable low bandgap diketopyrrolopyrrole (DPP) based derivatives: novel acceptors for organic solar cells, *J. Mater. Chem.* **2010**, *20*, 3626–3636.

(29) Walker, B.; Tamayo, A. B.; Dang, X.; Zalar, P.; Seo, J. H.; Garcia, A.; Tantiwiwat, M.; Nguyen, T. Nanoscale phase separation and high photovoltaic efficiency in solution-processed, small=molecule bulk heterojunction solar cells, *Adv. Funct. Mater.* **2009**, *19*, 3063–3069.

(30) Lee, C.; Lu, H.; Lan, C.; Huang, Y.; Liang, Y.; Yen, W.; Liu, T.; Lin, T.; Diau, E. W.; Yeh, C. Novel zinc porphyrin sensitizers for dye-sensitized solar cells: synthesis and spectral, electrochemical and photovoltaic properties, *Chem. Eur. J.* **2009**, *15*, 1403–1412.

(31) Campbell, W. M.; Jolley, J. W.; Wagner, P.; Wagner, K.; Walsh, P. J.; Gordon, K. C.; Schmidt-Mende, L.; Nazeeruddin, M. K.; Wang, Q.; Grätzel, M.; Officer, D. L. Highly efficient porphyrin sensitizers for dye-sensitized solar cells, *J. Phys. Chem. C* **2007**, *111*, 11760–11762.

(32) Zhu, X. Y.; Yang, Q.; Muntwiler, M. Charge-transfer excitons at organic semiconductor surface and interfaces, *Acc. Chem. Res.*, **2009**, *42*, 1779–1787.

(33) Coakley, Kevin M.; McGehee, Michael D. Conjugated polymer photovoltaic cells, *Chem Mater*, **2004**, *16*, 4533–4542

(34) Umemoto, Y.; Le, Y.; Saeki, A.; Seki, S.; Tagawa, S.; Aso, Y. Electronegative oligothiophenes fully annelated with hexafluorocyclopentene: synthesis, properties, and intrinsic electron mobility, *Org. Lett.*, **2008**, *10* (6), 1095-1098

(35) Peet, J.; Heeger, A. J.; Bazan, G. C. "Plastic" solar cells: self-assembly of mulk heterojunction nanomaterials by spontaneous phase separation, *Acc. Chem. Res.* **2009**, *42*, 1700–1708.

(36) Beck, Waldo J. E.; Wienk, Martijn M.; Janssen, René A. J. Hybrid solar cells from regioregular polythiophene and ZnO nanoparticles, *Adv. Funct. Mater.*, **2006**, *16*, 1112–1116

(37) Liu, Jinsong; Tanaka, Toru; Sivula, Kevin; Alivisatos, A. Paul; Fréchet, Jean M. J. Employing end-functional polythiophene to control the morphology of nanocrystal-polymer composites in hybrid solar cells, *J. Am. Chem. Soc.*, **2004**, *126*, 6550–6551

(38) Argazzi, Roberto; Bignozzi, Carlo A.; Heimer, Todd A.; Castellano, Felix N.; Meyer, Gerald J. Long-lived photoinduced charge separation across nanocrystalline TiO_2 interfaces, *J. Am. Chem. Soc.*, **1995**, *117*, 11815–11816

(39) Bair, J. S.; Harrison, R. G. Synthesis and optical properties of bifunctional thiophene molecules coordinated to ruthenium, *J. Org. Chem.* **2007**, *72*, 6653–6661.